Chaperone-mediated ordered assembly of the SAGA transcription complex

Alberto Elías-Villalobos[1], Damien Toullec[1], Céline Faux[1], Gwendaline Lledo[1], Martial Séveno[2], and Dominique Helmlinger[1,*]

[1]CRBM, CNRS, University of Montpellier, Montpellier, France

[2]BioCampus Montpellier, CNRS, INSERM, University of Montpellier, Montpellier, France

*Corresponding author: Dominique Helmlinger

Phone: +33-434-35-95-48

Fax: +33-434-35-94-10

Email: dhelmlinger@crbm.cnrs.fr

Running title: Principles of SAGA complex assembly

Keywords: Transcription, Chromatin, Multimeric complex, Chaperone

Abstract

Transcription initiation involves the coordinated activities of large multimeric complexes. Little is known about the mechanisms and pathways that drive their assembly from individual components. We report here several principles underlying the assembly of the highly conserved SAGA co-activator complex, which is composed of 19 subunits organized into functional modules. First, we demonstrate that SAGA assembles through an ordered pathway, in which the core subunit Spt20 recruits Tra1, which then promotes the incorporation of the de-ubiquitination module (DUB). Second, affinity purifications and phenotypic analyses identified a small region of Spt20 that is both necessary and sufficient to anchor Tra1 to SAGA. Third, Tra1 is shared with the NuA4 co-activator complex and is the only pseudokinase of the PIKK family. We accumulated functional and biochemical evidence that Tra1 shares a specific Hsp90 cochaperone with PIKKs, the Triple-T complex, for its cotranslational folding and *de novo* incorporation into both SAGA and NuA4. Finally, in contrast to its specific role in SAGA assembly, Tra1 contributes to scaffold the entire NuA4 complex. Overall, our study brings mechanistic insights into the *de novo* assembly of transcriptional complexes via ordered pathways and reveals the contribution of dedicated chaperones to this process.

Introduction

A critical step in gene expression is transcription initiation, which is controlled by many factors that typically function as part of multimeric, multifunctional complexes. Genetic, biochemical, and structural evidence indicate that their subunits form distinct modules with specific functions and numerous studies have characterized their regulatory activities and roles in gene expression. In contrast, much less is known about how these complexes assemble, which chaperones are required, and whether their assembly can be modulated to control or expand their functions. Deciphering these principles is, however, important to understand their structural organization, function, and allosteric regulation (Marsh and Teichmann, 2015). Notably, chromatin-modifying and –remodeling complexes often share functional modules and therefore probably require dedicated mechanisms and chaperones for proper assembly (Helmlinger and Tora, 2017).

One such complex, the Spt-Ada-Gcn5 acetyltransferase (SAGA) co-activator, bridges promoter-bound activators to the general transcription machinery. In yeast, SAGA is composed of 19 subunits, which are organized into five modules with distinct regulatory roles during transcription (Koutelou et al., 2010; Spedale et al., 2012). These include histone H3 acetylation (HAT), histone H2B de-ubiquitination (DUB), and regulation of TBP recruitment at core promoters. A fourth module consists of a set of core subunits that scaffold the entire complex, most of which are shared with the general transcription factor TFIID. Finally, its largest subunit, Tra1, directly binds to a diverse range of transcription factors. Tra1 is shared with another transcriptional co-activator complex, yeast NuA4, which also contains a HAT module that preferentially targets histone H4 and the H2A.Z variant (Lu et al., 2009). Genetic and biochemical studies indicate that Tra1 primary role is to recruit SAGA and NuA4 to specific promoters upon activator binding. It has been difficult, however, to define the specific contribution of Tra1 to SAGA and NuA4 regulatory roles in transcription.

The fission yeast *Schizosaccharomyces pombe* provides a unique opportunity to address this issue because it has two paralogous proteins, Tra1 and Tra2, and each has

non-redundant roles that are specific for SAGA and NuA4, respectively (Helmlinger, 2012). Within SAGA, Tra1 has specific regulatory roles and minor effects on complex assembly (Helmlinger et al., 2011), consistent with its peripheral position in the recent cryo-electron microscopy structure of yeast SAGA (Sharov et al., 2017). In contrast, a recent partial structure of the yeast NuA4 complex indicates that Tra1 occupies a more central position and contributes to scaffold the entire complex (Wang et al., 2018). However, little is known about how Tra1 assembles into the SAGA and NuA4 complexes, whether it involves similar or distinct mechanisms, and which chaperones are required.

Yeast Tra1 and its human ortholog, TRRAP, belong to a family of atypical kinases, the phosphoinositide 3 kinase-related kinases (PIKKs), but lack catalytic residues and therefore classify as pseudokinases (McMahon et al., 1998; Saleh et al., 1998; Vassilev et al., 1998). The reason for the evolutionary conservation of a typical PIKK domain architecture within Tra1 orthologs remains elusive. Although active PIKKs are implicated in diverse processes, they share a dedicated HSP90 cochaperone, the Triple T complex (TTT), for their stabilization, maturation, and incorporation into active complexes (Anderson et al., 2008; Hurov et al., 2010; Izumi et al., 2012; Kaizuka et al., 2010; Takai et al., 2010, 2007). TTT was initially discovered in fission yeast and is composed of three conserved, specific subunits, Tel2, Tti1, and Tti2 (Hayashi et al., 2007; Shevchenko et al., 2008; Takai et al., 2010). Numerous functional studies in different organisms have implicated TTT in PIKK signaling in response to DNA damage or metabolic stress (Ahmed et al., 2001; Anderson et al., 2008; Hoffman et al., 2016; Hurov et al., 2010; Izumi et al., 2012; Kaizuka et al., 2010; Kim et al., 2012; Shikata et al., 2007; Takai et al., 2007). In contrast, the effect of TTT on the Tra1 pseudokinase, the only inactive PIKK, remains poorly understood, despite evidence that TTT components interact physically and genetically with Tra1 in yeast (Genereaux et al., 2012; Hayashi et al., 2007; Helmlinger et al., 2011; Inoue et al., 2017; Shevchenko et al., 2008) and stabilize TRRAP in human cells (Hurov et al., 2010; Izumi et al., 2012; Kaizuka et al., 2010; Takai et al., 2007).

Here, using proteomic, biochemical, and genetic approaches, we present evidence that *S. pombe* TTT is required for the incorporation of Tra1 into SAGA and Tra2 into NuA4 and contributes to their functions in gene expression. In contrast to Tra1 within SAGA, we demonstrate that Tra2 has a general scaffolding role in NuA4 assembly, consistent with recent structural and biochemical observations (Wang et al., 2018). Mechanistically, structure-guided mutational analyses identified the residues of Tra1 that direct its specific interaction with SAGA. Furthermore, affinity purifications revealed that a small region of the core subunit Spt20 constitutes the major interaction interface between Tra1 and SAGA. Finally, we establish that the incorporation of the de-ubiquitination module (DUB) follows that of Tra1, uncovering an ordered assembly pathway for the SAGA complex. Overall, our work brings mechanistic insights into the assembly and modular organization of an important transcriptional co-activator complex and defines the topology of the Tra1-SAGA interface.

Results

Proteomic characterization of the TTT complex from *S. pombe*.

The fission yeast *S. pombe* offers a unique opportunity to study the specific roles of Tra1 within either SAGA or NuA4. To address the contribution of the Hsp90 cochaperone TTT in Tra1-dependent gene expression, we first performed an unbiased characterization of the TTT complex. For this, *S. pombe* Tel2, Tti1, and Tti2 were subjected to tandem affinity purification (TAP) followed by quantitative mass spectrometry analyses (MS). Consistent with previous studies in fission yeast and mammalian cells (Hayashi et al., 2007; Takai et al., 2010), Tti2 interacts with Tel2 and Tti1 almost stoichiometrically (Figure 1A). Interestingly, Tti2 pulls down significant amounts of Asa1, a protein previously identified in Rvb1 purifications from both *S. cerevisiae* and *S. pombe* (Shevchenko et al., 2008) and involved in PIKK stabilization (Goto et al., 2017; Rozario and Siede, 2012; Stirling et al., 2011). In contrast, the AAA+ ATPase Rvb1 and Rvb2 were detected with poorer specificity and reproducibility in Tti2 purifications, suggesting weaker or more transient interaction. The Hsp70 and Hsp90 chaperones were not specifically detected in Tti2 purifications, as compared to a negative control, likely because of their high abundance in protein extracts. Similar observations were made in MS analyses of Tel2 and Tti1 purifications (Figure S1).

Additionally, most PIKKs were specifically and reproducibly enriched in Tti2, Tel2, and Tti1 purifications, including both *S. pombe* Tra1^{TRRAP} orthologs, Tra1 and Tra2 (Figure 1A and Figure S1). We observed either no or weak interaction with Tel1^{ATM} and Rad3^{ATR}, respectively, possibly because of low DNA damage signaling in exponentially growing cells. Importantly, we did not detect any subunit from the mature complexes into which PIKKs eventually incorporate and become active, except Wat1^{Lst8}, a component of both mTOR-containing complexes, TORC1 and TORC2 (Figure 1B). Altogether, these quantitative MS analyses indicate that Tti2, Tel2, and Tti1, together with Asa1, form a stable multimeric complex that interacts with most PIKKs in *S. pombe*, particularly Tra1^{TRRAP}, Tra2^{TRRAP}, Tor1^{mTOR}, and Tor2^{mTOR} (Figure 1B).

The TTT subunit Tti2 contributes to Tra1 and Tra2 function in gene expression.

In human cells, TTI2 is critical for the stability of both TEL2 and TTI1 at steady state (Hurov et al., 2010), in agreement with its stable association within the TTT complex. We thus focused our analysis of TTT function in Tra1- and Tra2-dependent gene expression to that of Tti2, which is essential for viability in *S. pombe* (Inoue et al., 2017). Deletion of *tra2*+ is also lethal, whereas *tra1*Δ mutants are viable (Helmlinger et al., 2011). Using a strategy based on inducible CreER-loxP-mediated recombination, we generated conditional knock-out alleles of *tti2*+ (*tti2-CKO*) and *tra2*+ (*tra2-CKO*). Both strains showed β-estradiol-induced loss of Tti2 or Tra2 expression, accompanied by progressive proliferation defects (Figures S2 and S3).

We then performed genome-wide expression analyses of DMSO- and β-estradiol-treated *tti2-CKO* and *tra2-CKO* cells, compared to a *cre-ER* strain treated identically. We also analyzed *tra1*Δ mutants that were compared to a wild-type strain. Differential expression analysis revealed specific and overlapping changes in each mutant (Figure S4A-D). For example, we confirmed down-regulation of the *SCC569.05c*$^{+}$ and *gst2*$^{+}$ genes in both *tti2-CKO* and *tra1*Δ mutants (Figure S4E) and of *SPCC1884.01*$^{+}$ and *SPCAC977.12*$^{+}$ in both *tti2-CKO* and *tra2-CKO* mutants (Figure S4F). To compare their overall transcriptome profiles, we performed hierarchical clustering of all differentially expressed genes and found all possible classes. These include genes which expression is up- or down-regulated in only one mutant, in two mutants, or in all three mutants (Figure 1C). A Venn diagram representation of all differentially expressed genes showed the extent of the overlap between all three mutants. Remarkably, 105 out of the 184 Tti2-dependent genes are also regulated by Tra1 (25 genes), Tra2 (72 genes), or both Tra1 and Tra2 (8 genes) (Figure 1D). Finally, Tra1 has important roles in recruiting SAGA and NuA4 to chromatin. We thus evaluated the effect of Tti2 on the binding of the SAGA subunit Spt7 and the NuA4 subunit Epl1 to specific promoters, using chromatin immunoprecipitation (ChIP). Upon depletion of Tti2, we observed reduced occupancy of Spt7 at the *pho84*+ and *mei2*+ promoters and of Epl1 at the *ssa2*+ promoter, despite normal steady-state levels (Figure 1E,F).

In conclusion, we accumulated functional evidence suggesting that Tti2, probably as part of the TTT complex, contributes to the regulatory activities of Tra1 and Tra2 in gene expression. Therefore, similar to their active counterparts, the Tra1 and Tra2 pseudokinases require the TTT cochaperone to function.

Tti2 promotes the *de novo* incorporation of Tra1 and Tra2 into SAGA and NuA4.

These observations prompted us to test whether Tti2, as a cochaperone, promotes the incorporation of Tra1 and Tra2 into SAGA and NuA4, respectively, as shown for human mTOR and ATR-containing complexes (Kaizuka et al., 2010; Takai et al., 2010). For this, we affinity purified SAGA and NuA4 upon conditional deletion of *tti2*+. Silver staining and quantitative MS analyses revealed a 10-fold reduction of Tra1 from SAGA when Tti2 is depleted, as compared to control conditions (Figure 2A). Similarly, we observed about a 2-fold reduction in the levels of Tra2 in purified NuA4 complexes (Figure 2B).

We next tested if Tti2 prevents Tra1 and Tra2 disassembly from their complex or, rather, promotes their *de novo* incorporation. For this, we took advantage of the viability of *tra1*Δ mutants and disrupted the *tra1*+ promoter with a transcription terminator sequence flanked by *loxP* sites (*RI-tra1*+, Figure S5A). With this allele, CreER-mediated recombination allows the inducible expression of Tra1 at endogenous levels. As a proof of principle, β-estradiol addition to *RI-tra1*+ strains restored their growth defects in conditions of replicative stress, using hydroxyurea (HU) (Figure S5A), to which *tra1*Δ mutants are sensitive (Helmlinger et al., 2011). Purification of SAGA from *RI-tra1*+ cells showed a time-dependent, progressive increase of Tra1 in Spt7 purification eluates upon β-estradiol addition, validating this approach for monitoring the *de novo* incorporation of Tra1 into SAGA (Figure S5B). However, to conditionally deplete TTT in *RI-tra1*+ cells, we had to develop a strategy different from the CreER-loxP-mediated knockout used so far. Fusing the TTT subunit Tel2 to an auxin-inducible degron (AID) allowed inducible degradation and subsequent proliferation defects by adding the plant hormone auxin (Figure S6A-C). Then, silver staining and quantitative MS analyses of SAGA purified from *RI-tra1*+ *tel2-AID* cells showed reduced

interaction between *de novo* produced Tra1 and affinity purified Spt7 in cells partially depleted of Tel2 (lane 2 *vs* 4, Figure 2C). These results demonstrate that TTT contributes to the *de novo* incorporation of Tra1 into the SAGA complex.

Work in human cells revealed that TTT functions as an adaptor, which recruits the HSP90 chaperone to PIKKs specifically (Izumi et al., 2012; Pal et al., 2014; Takai et al., 2010). We thus determined if the *de novo* incorporation of Tra1 into SAGA requires Hsp90 in *S. pombe*. To test this, we first tested the effect of the conditional inactivation of Hsp90 on SAGA subunit composition at steady state. For this, we affinity purified Spt7 from *hsp90-26* mutants grown at either permissive or restrictive temperature (Aligue et al., 1994). Silver staining analysis showed that Hsp90 inactivation caused a specific decrease of Tra1 in Spt7 purification eluates (Figure S7). To minimize the impact of Hsp90 on CreER activity, we next assessed the *de novo* incorporation of Tra1 into SAGA using *hsp90-201* mutants, which harbor a weaker Hsp90 mutant allele (Alaamery and Hoffman, 2008). Silver staining and quantitative MS analyses revealed a decrease of newly synthesized Tra1 in SAGA purified from *hsp90-201* mutants, as compared to wild-type cells (lane 4 *vs* 2, Figure 2D). Although we observed a modest effect in this experimental condition, this result is consistent with our interpretation that Hsp90, like TTT, contributes to the *de novo* incorporation of Tra1 into SAGA. Altogether, these data indicate that, similar to its activity on mTOR- and ATR-containing complexes, TTT acts as an Hsp90 cochaperone that promotes the assembly of Tra1 into SAGA and presumably of Tra2 into NuA4. Therefore, pseudokinases and kinases of the PIKK family share a specific, dedicated chaperone machinery for their maturation and incorporation into active complexes.

Tra1 and Tra2 have distinct structural roles between SAGA and NuA4.

We noted that the absence of Tti2 affected SAGA and NuA4 differently. Upon Tti2 depletion, the decrease of Tra1 does not affect SAGA overall migration profile, similar to what we observed in a *tra1*Δ mutant (Figure 2A) (Helmlinger et al., 2011). In contrast, the effect of Tti2 on Tra2 incorporation within NuA4 is less pronounced, but seems to cause a global

decrease in the amount of purified NuA4 (Figure 2B). We reasoned that the bait used, the Mst1 HAT subunit, might dissociate from the rest of the complex upon *tti2+* deletion and loss of Tra2.

To directly evaluate the effect of Tra2 on NuA4 subunit composition, we purified NuA4 upon *tra2+* deletion, using *tra2-CKO* cells. For this, we affinity purified either Epl1, which anchors the HAT module to the rest of NuA4 in *S. cerevisiae* (Boudreault et al., 2003), or Vid21, which *S. cerevisiae* ortholog Eaf1 is a platform for NuA4 assembly (Auger et al., 2008). Silver staining and quantitative MS analyses of affinity purified Mst1, Epl1, and Vid21 revealed that each interact with a similar set of 13 proteins that define the NuA4 complex from *S. pombe* (Figure S8A-C), in agreement with a previous study (Shevchenko et al., 2008). Upon the loss of Tra2, we observed an overall decrease in the amount of purified NuA4, using either Epl1 or Vid21 as baits (Figure 2E). Quantitative MS analyses of Vid21 purification eluates confirmed an overall decrease of all 13 NuA4 subunits upon the loss of Tra2 (Figure 2F). Altogether, our biochemical analyses indicate that, in contrast to Tra1 in SAGA, Tra2 contributes to the scaffolding and stabilization of the entire NuA4 complex. These distinct structural roles are consistent with the peripheral position of Tra1 within SAGA (Sharov et al., 2017) and the central position in NuA4 structure (Wang et al., 2018).

Cotranslation interaction between the TTT cochaperone and its clients Tra1 and Tra2.

Next, we asked if TTT contributes to SAGA and NuA4 functions directly, by controlling the incorporation of Tra1 and Tra2 at specific promoters. However, ChIP revealed no enrichment of Tel2 over background at SAGA- (*mei2+*) and NuA4-bound promoters (*ssa2+*) (Figure 3A). Furthermore, fluorescent microscopy analysis of endogenous Tel2 tagged with GFP showed a clear depletion form the nucleus (data not shown).

We hypothesized that, rather than acting at chromatin, TTT might recognize newly synthesized Tra1 and Tra2 to promote their folding and maturation, either before or concomitantly with their complex incorporation. To test this possibility, we performed RNA immunoprecipitations (RIP) of TTT. Although TTT subunits do not contain RNA-binding

motifs and thus presumably do not bind RNA directly, previous work has shown that RIP can detect cotranslational interactions between a protein and a nascent polypeptide (Duncan and Mata, 2014, 2011).

Conventional and quantitative PCR analyses revealed a specific enrichment of the *tra1*+ mRNA in RIPs of all three TTT subunits, Tel2, Tti1, and Tti2, as compared to several negative controls (Figure 3B). These include an unrelated mRNA, *isp6*+, a strain lacking the epitope tag used to RIP TTT (no HA), and a strain in which the same tag was fused to the TORC2 subunit Ste20^{Rictor} (Figure 3B). We observed a comparable enrichment of the *tra2*+ mRNA in purified Tti1. In addition, the presence of an intron within *tra2*+ allowed us to show that Tti1 binds only the mature form of *tra2*+, and not its pre-mRNA (Figure 3C). Then, we repeated Tti1 RIPs in cells either briefly treated with an inhibitor of translation elongation, puromycin, or using EDTA to dissociate ribosomes. Both treatments abolished Tti1 binding to *tra1*+ and *tra2*+ mRNAs (Figure 3C). We conclude that the interaction between TTT and these mRNAs requires ribosomal integrity and activity and therefore occurs cotranslationally.

We then tested whether TTT binds exclusively to the nascent Tra1 and Tra2 polypeptides or, rather, recognizes other SAGA and NuA4 subunits to promote their cotranslational assembly. For this, we probed Tel2 and Tti2 RIPs for the presence of mRNAs encoding the SAGA core subunits Ada1, Taf12, and Spt20, as well as the NuA4 subunits Vid21, Epl1, and Eaf7. Besides *tra1*+ and *tra2*+, Tel2 or Tti2 did not bind any of the other mRNAs tested (Figure 3D,E), indicating cotranslational binding of TTT to its PIKK clients, Tra1 and Tra2, but not to their interaction partners. Consistent with this result, SAGA and NuA4 subunits were not detected in our MS analyses of TTT purifications (Table S1). Conversely, no TTT subunits were detected in MS analyses of purified SAGA, except in Tra1 purifications (Figure S9A).

Recent work revealed widespread cotranslational assembly of protein complexes (Shiber et al., 2018), including *S. cerevisiae* SAGA (Kassem et al., 2017). In marked contrast, we did not observe evidence for cotranslational assembly of Tra1 and Tra2 into

SAGA and NuA4, respectively. Indeed, RIP of the SAGA subunit Spt20 and the NuA4 subunit Epl1 failed to enrich the *tra1*+ and *tra2*+ mRNAs, as compared to Tti2 and no tag controls (Figure 3F). Thus, the nascent Tra1 and Tra2 polypeptides interact specifically with TTT, but not with their interacting partners within SAGA and NuA4. Altogether, these data indicate that TTT recognizes Tra1 and Tra2 early during their biogenesis, cotranslationally, but is not directly involved in promoting interaction with their partners within each complex.

The TTT cochaperone recognizes Tra1 in a prefolded state.

To gain further insights into the mechanism by which TTT promotes Tra1 folding and maturation, prior to its incorporation into SAGA, we performed a structure-function analysis of Tra1-TTT and Tra1-SAGA interactions. We serendipitously observed that C-terminal tagging of Tra1 impairs its interaction with SAGA but not with TTT (Figure S9B), whereas N-terminally tagged Tra1 efficiently pulled down both SAGA and TTT (Figure S9A).

The C-terminal end of Tra1 consists of the small FATC domain, which is a distinctive feature of PIKKs. We thus investigated how this domain contributes to the TTT-dependent incorporation of Tra1 into SAGA. It is characterized by the presence of highly conserved, large hydrophobic residues, particularly the last two amino-acids (Figure 4A) (Lempiäinen and Halazonetis, 2009). Recent structures of PIKKs showed that the FATC is an integral part of the kinase domain, inserted close to the active site (Imseng et al., 2018). Truncating *tra1*+ from its 3' end confirmed that the FATC is essential for Tra1 to interact with SAGA, as observed in silver staining and quantitative MS analyses of SAGA purifications (Figure 4A,B). A mutant form of Tra1 (Tra1-AA), in which only the last two hydrophobic residues are substituted with alanine, is also absent from SAGA purifications (Figure 4A,B). We verified that the steady-state levels of all Tra1 mutants were comparable to wild-type Tra1 (Figure S10A,B). Phenotypic analyses of *tra1-AA* mutants, as well as of strains carrying single *tra1-WA* and *tra1-AL* mutations, showed that all *tra1* FATC mutants are sensitive to replicative stress, similar to *tra1*Δ mutants (Figure 4C). Finally, RNA-seq analyses of *tra1-AA* and *tra1*Δ mutants revealed a strong correlation between the transcriptomic changes observed in each

strain, as compared to a wild-type control (r^2 = 0.75) (Figure 4D). Likewise, we replaced the two C-terminal residues from Tra2 FATC with alanine in a diploid strain, generating *tra2+*/*tra2-AA* heterozygotes. Their sporulation showed a 2:2 segregation of a lethality phenotype and the genotype of all viable spores was *tra2+* (Figure S11), similar to *tra2+*/*tra2*Δ diploids (Helmlinger et al., 2011). Overall, these results indicate that the FATC domain is critical for Tra1 and Tra2 functions, although both pseudo-PIKKs lack all catalytic residues.

Contrary to its essential role in SAGA incorporation, quantitative MS analyses of purified TTT showed that the FATC domain does not contribute to Tra1 interaction with TTT. Indeed, we detected comparable levels of Tra1 in Tti2 purification eluates from strains in which the FATC is either mutated (*tra1-AA*) or truncated (*tra1-1*) (Figure 4E). In contrast, analysis of *tra1-2*, *tra1-3*, and *tra1-4* mutants showed that Tti2 did not interact with any of the shorter C-terminal truncations of Tra1 (Figure 4E), suggesting that Tti2 recognizes Tra1 PI3K domain. Accordingly, RIP of Tti2 in *tra1-2* and *tra1-4* mutants showed that Tti2 did not bind the mRNA of *tra1+* mutants lacking the PI3K domain (Figure 4F), reinforcing our conclusion that TTT primarily binds Tra1 cotranslationally.

To conclude for this part, protein and RNA affinity purifications demonstrate that TTT binds the nascent PI3K domain of Tra1, but that the C-terminal FATC domain of Tra1 is critical for its incorporation into SAGA. TTT might thus bind and chaperone a prefolded form of Tra1 during translation, because folding into a conformation that recognizes SAGA can only occur when ribosomes reach the end of *tra1+* mRNA and synthesize the C-terminal, FATC residues. Supporting this possibility, cycloheximide chase revealed that the Tra1-AA mutant protein is degraded faster than wild-type Tra1 (Figure 4G), suggesting that a Tra1 FATC mutant is misfolded and targeted for degradation. Accordingly, the half-life of human TRRAP or *S. cerevisiae* Tra1 decreases upon conditional knockout of TEL2 or mutation of its last residue, respectively (Genereaux et al., 2012; Takai et al., 2007).

Mechanism governing the specific incorporation of Tra1 into SAGA.

Although the FATC domain is essential for Tra1 to incorporate into SAGA (Figure 4), it is unlikely to define the specificity of Tra1 binding to SAGA because the FATC is also essential for Tra2. In addition, the most recent cryo-electron microscopy structure of *Pichia pastoris* SAGA suggests that another region of Tra1 directly contacts SAGA (Figure 5A) (Sharov et al., 2017). Resolution of the secondary structure elements of Tra1 bound to SAGA identified a narrow and highly flexible hinge region that was suggested to form the major, if not the single interaction surface between Tra1 and SAGA. This region is located near the start of Tra1 FAT domain and consists of about 50 residues that fold into 3 distinct α-helices (H1-H3, Figure 5A). Multiple alignments of Tra1 orthologs from yeast, invertebrate, and vertebrate species indicate that this region is conserved throughout eukaryotes (Figure 5A). Interestingly, the homologous region of *S. pombe* Tra2, which binds NuA4 only (Figure 2B), is more divergent and has therefore the potential to define SAGA binding specificity.

Deletion of a few helices within Tra1 might cause important structural rearrangements and destabilize the protein (Knutson and Hahn, 2011). To determine the contribution of this region to Tra1-SAGA interaction, we swapped these 50 residues with that from Tra1 closest PIKK, *S. pombe* Tra2, which is not present in SAGA (Figure 5B). We also introduced the sequence from *S. cerevisiae* Tra1, which interacts with both SAGA and NuA4. Both Tra1-ScTra1 and Tra1-SpTra2 mutant proteins were expressed at levels similar to those of wild-type Tra1 (Figure 5C). In marked contrast, silver staining and quantitative MS analyses revealed that the Tra1-SpTra2 hybrid is not detectable in Spt7 purifications, whereas normal levels of the Tra1-ScTra1 hybrid were observed (Figure 5C). Similarly, a Tra1-mTOR hybrid protein is unable to co-purify with SAGA (Figure S12A), consistent with human mTOR assembling into different PIKK-containing complexes, TORC1 and TORC2. Importantly, both Tra1-ScTra1 and Tra1-SpTra2 hybrid proteins efficiently copurified with Tti2, as shown by quantitative MS analyses (Figure S12B). Thus, this region does not affect Tra1 binding to TTT and Tra1-SpTra2 is normally recognized by its cochaperone despite being defective in SAGA incorporation.

Phenotypic analyses of *tra1-Sctra1* and *tra1-Sptra2* strains revealed that *tra1-Sptra2* mutants are sensitive to replicative stress and caffeine, similar to *tra1*Δ mutants, whereas *tra1-Sctra1* strains showed no growth defects, as compared to wild-type cells (Figure 5D). RNA-seq analyses of *tra1-Sctra1* and *tra1-Sptra2* strains mutants revealed a positive correlation between the transcriptomic changes observed in *tra1-Sptra2* and *tra1*Δ mutants, as compared to a wild-type control (r^2 = 0.58) (Figure 5E). In contrast, *tra1-Sctra1* mutants showed little gene expression changes, which correlated poorly with those observed in *tra1*Δ mutants (r^2 = 0.16) (Figure 5F). Thus, a 50-residue region from *S. cerevisiae* Tra1 complements that of *S. pombe* Tra1, likely because *S. cerevisiae* Tra1 is present in both SAGA and NuA4. In contrast, the homologous *S. pombe* Tra2 region is more divergent and does not complement that of *S. pombe* Tra1 because Tra2 binds NuA4 specifically, possibly through other regions. Altogether, structural, biochemical and functional evidence demonstrate that Tra1 directly contacts SAGA through a restricted, 50-residue region from the FAT domain. This region of Tra1 consists of 3 α-helices that fold into a cup-shaped structure (Figure 5A) (Sharov et al., 2017). We thus coined this part of the Tra1-SAGA hinge as the Cup SAGA Interacting (CSI) region of Tra1.

The SAGA subunit Spt20 is necessary and sufficient for anchoring Tra1 into SAGA.

Patrick Schultz's laboratory reported that the hinge accommodates a putative α-helix belonging to a SAGA subunit other than Tra1 (Sharov et al., 2017). This observation encouraged us to identify the residues that forms the head part of the hinge and directly contacts Tra1 CSI region. Besides Tra1, there are 18 subunits in *S. pombe* SAGA (Helmlinger et al., 2008). Genetic, biochemical, and structural evidence suggest that, of these, Ada1, Taf12, and Spt20 are good candidates to anchor Tra1 within SAGA (Han et al., 2014; Helmlinger et al., 2011; Lee et al., 2011; Setiaputra et al., 2015; Sharov et al., 2017; Wu and Winston, 2002). Silver staining analyses revealed that Tra1 is undetectable in SAGA purified from *spt20*Δ mutants, without any other visible changes in its overall migration profile (Figure 6A). *S. pombe* Spt20 is thus essential to incorporate Tra1 into SAGA.

In *S. pombe*, Spt20 is 474 residue long and can be divided into an N-terminal half that contains several conserved regions, named homology boxes (HB) (Nagy et al., 2009) and a C-terminal low-complexity region (LCR) (Figure 6B). Deletion of Spt20 N-terminal half (residues 1-255) abolished its interaction with SAGA (data not shown), indicating that this portion of Spt20 mediates its binding to the complex. Silver staining analyses of SAGA purified from mutants that remove various lengths of Spt20 C-terminal LCR identified a short region of 11 residues that is crucial to incorporate Tra1 into SAGA (Figure 6B). Quantitative MS analyses confirmed that Tra1 does not interact with SAGA in *spt20-290* mutants, in which residues 291-474 are deleted, whereas normal levels of Tra1 are detected in *spt20-300* mutants, in which residues 301-474 are deleted (Figure 6B). Structure prediction of *S. pombe* Spt20 identified a α-helix in this region, which we coined the Head Interacting with Tra1 (HIT) (Figure 6C). Silver staining and quantitative MS analyses of SAGA purified from mutants in which Spt20 HIT region is deleted (*spt20-HIT*Δ) confirmed the importance of this region for Tra1 interaction (Figure 6C). Similarly, mutational analyses of the HIT identified 4 residues, FIEN, that are important for Tra1 incorporation into SAGA, whereas the next 4, positively charged RRKR residues contribute less (Figure 6C). All Spt20 truncation, deletion, and point mutants were expressed at levels comparable to those of wild-type Spt20 (Figure S13) and, importantly, were present in purified SAGA complexes (* in Figure 6B,C).

We next evaluated the phenotype of *spt20-HIT* mutant strains. Similar to *tra1*Δ mutants, *spt20-HIT*Δ and *spt20-FIEN* mutants showed sensitivity to replicative stress, whereas *spt20-RRKR* showed milder defects, as compared to wild-type cells (Figure 6D). We then performed RNA-seq analyses of *spt20*Δ and *spt20-HIT*Δ mutants and paralleled the transcriptomic changes with those observed in *tra1-Sptra2* and *tra1*Δ mutants, as compared to a wild-type control strain. First, comparing *spt20-HIT*Δ with *spt20*Δ mutants revealed that Spt20 HIT region contributes to the expression of only a subset of Spt20-dependent genes (r^2 = 0.35) (Figure 6E), consistent with the HIT region specifically involved in Tra1 interaction. Indeed, comparing *spt20-HIT*Δ with *tra1*Δ mutants resulted in a better correlation

(r^2 = 0.44) (Figure 6F). Remarkably, the best correlation was obtained when comparing *spt20-HIT*Δ with *tra1-Sptra2* mutants (r^2 = 0.62) (Figure 6G), *ie* strains in which the hinge is mutated on either side of the same interaction surface. Altogether, biochemical and functional approaches identified a narrow region of Spt20 which is necessary to incorporate Tra1 into SAGA, likely by direct interaction with Tra1 CSI region.

Finally, we asked whether Spt20 HIT region is sufficient to interact with Tra1. For this, a 40-residue peptide encompassing the HIT region was immobilized, through fusion to GST, and incubated with *S. pombe* protein extracts prepared from wild-type, *tra1-Sptra2* and *tra1-Sctra1* strains. The GST-HIT specifically pulled down wild-type *S. pombe* Tra1 and the Tra1-ScTra1 hybrid protein, as compared to GST alone (lanes 1 *vs* 2 and 5 *vs* 6, Figure 6H). Consistent with *in vivo* observations that Tra1 CSI region mediates interaction with Spt20, lower amounts of the Tra1-SpTra2 hybrid protein were recovered on the GST-HIT column, although we detected some binding compared to GST alone (lane 3 *vs* 4, Figure 6H). Overall, these experiments indicate that Spt20 HIT region folds into a α-helix that is both necessary and sufficient for binding to Tra1. We have thus deciphered the molecular topology of the narrow hinge that mediates Tra1-SAGA contacts. Remarkably, only a few residues are involved on each side of the SAGA-Tra1 interface, in agreement with the peripheral position of Tra1 within SAGA (Sharov et al., 2017).

Tra1 orchestrates an ordered pathway for SAGA assembly.

Throughout this study, quantitative MS analyses of SAGA purified from various mutants revealed an unexpected finding. Indeed, the amount of DUB module subunits within SAGA consistently decreased when Tra1 was not incorporated into the complex. For instance, we measured a reproducible decrease of both Sgf73 and Ubp8 in Spt7 purified from *tra1*Δ or β-estradiol-treated *tti2-CKO* cells, as compared to control conditions (Figure 7A,B). Similarly, mutating either side of the hinge reduced the amount of both Sgf73 and Ubp8 in SAGA purifications, as shown in *spt20-290*, *spt20-HIT*Δ, *spt20-FIEN*, and *tra1-Sptra2* cells ('Hinge*' in Figure 7A,B). In contrast, the levels of Sgf73 and Ubp8 did not change in Spt7

purifications from *spt20-300*, *spt20-RRKR* and *tra1-Sctra1* cells, in which Tra1 incorporates into SAGA (data not shown). The other two DUB subunits, Sgf11 and Sus1, are about 10 kDa and therefore less reliably quantified by MS. Still, the reproducibility of this effect across distinct mutants that all affect Tra1 incorporation suggested that Tra1 promotes the assembly of the DUB module into SAGA.

We first asked whether, conversely, the DUB stabilizes Tra1 within SAGA. In *S. cerevisiae*, Sgf73 is critical to anchor the DUB module into SAGA (Köhler et al., 2008). Mass spectrometry analyses confirmed that, in *S. pombe sgf73*Δ mutants, the DUB subunits Ubp8, Sgf11, and Sus1 were absent from SAGA purifications (data not shown). In contrast, silver staining and MS analyses indicated that Spt20 and Tra1 incorporation into SAGA was similar between wild-type and *sgf73*Δ strains (Figure 7C). Altogether, these results suggest that SAGA assembly follows a directional, ordered pathway, in which Spt20 anchors Tra1, which then stabilizes the DUB into SAGA.

To test this hypothesis directly, we purified SAGA from *RI-tra1+* strains (Figure S5), in which we tagged endogenous Sgf11 with a MYC epitope. We then concomitantly monitored the kinetics of the *de novo* incorporation of Tra1 and the DUB module into SAGA. First, we confirmed that Sgf11 interacts less strongly with Spt7 in *tra1*Δ mutants or untreated *RI-tra1+* cells, as compared to control conditions (lanes 2 and 3 *vs* 6, Figure 7D). Second, we detected a progressive increase in the amount of Sgf11 that interacts with Spt7 upon β-estradiol treatment and *de novo* incorporation of Tra1 into SAGA (lanes 4 and 5, Figure 7D). Quantification of independent experiments confirmed these observations (Figure 7E). Comparison of the relative levels of Sgf11 and Tra1 in SAGA at 4 hours suggested that the assembly of the DUB module is slightly delayed, as compared to Tra1.

Overall, we accumulated functional and biochemical evidence that support a model in which, prior to assembly into SAGA, the nascent Tra1 polypeptide is bound by the TTT cochaperone, most likely to promote its folding into a mature conformation. Tra1 is

assembled by direct interaction with a narrow region of Spt20 and then promotes the incorporation of the DUB module within SAGA (Figure 7F).

Discussion

Many chromatin and transcription regulators function within large multimeric complexes, but little is known about their assembly. Our work brings several mechanistic insights into the *de novo* assembly and modular organization of one such complex, the SAGA transcriptional co-activator (Figure 7F). First, functional and biochemical evidence indicate that the Hsp90 cochaperone, TTT, promotes the folding and maturation of nascent Tra1 polypeptides during translation, prior to incorporation into SAGA. Notably, the paralogous NuA4-specific subunit Tra2 assembles through a similar mechanism. Second, structure-guided mutational analyses defined the topology of the Tra1-SAGA interface, which is restricted to a single α-helix of the core subunit Spt20 contacting a small, 50-residue region of Tra1. Third, we identified an ordered assembly pathway of SAGA, by which Tra1 interacts with Spt20 and then stabilizes the DUB module within the complex.

Chaperone-mediated cotranslational folding of Tra1 and Tra2 precedes assembly.

Many proteins function as part of multimeric complexes and describing the principles that govern their assembly is key to understand their structural organization, function, and regulation. Seminal work revealed that complexes are generally assembled by ordered pathways that appear evolutionarily conserved (Marsh and Teichmann, 2015). Cotranslational assembly has emerged as a prominent regulatory mechanism for promoting protein-protein interactions and the building of a complex (Duncan and Mata, 2011; Shiber et al., 2018; Shieh et al., 2015). Specifically, cotranslational interactions were observed for the SET1C histone methyltransferase complex (Halbach et al., 2009) and, more recently, between specific SAGA subunits (Kamenova et al., 2018; Kassem et al., 2017). Finally, a recent study demonstrated that Taf5, which is shared between SAGA and the general transcription factor TFIID, require a dedicated chaperone, the CCT chaperonin, for incorporation into pre-assembly modules (Antonova et al., 2018). Our study therefore contributes to the emerging concept that dedicated chaperone machineries control the ordered assembly of chromatin and transcription regulatory complexes.

Importantly, however, we observed cotranslational binding of the TTT cochaperone to Tra1 and Tra2, but not to any other SAGA or NuA4 components. Conversely, neither SAGA nor NuA4 appear to interact with Tra1 or Tra2 cotranslationally. Thus, TTT recognizes its clients early upon synthesis and prior to assembly into SAGA or NuA4. Shiber and colleagues recently reported that complexes requiring specific chaperones and assembly factors are less likely to assemble cotranslationally (Shiber et al., 2018). As predicted from their observations, we propose that some complexes, or specific subunits, require the cotranslational function of assembly factors, rather than binding partners. Here, Tra1 and Tra2 would require cotranslational chaperoning activity, instead of binding of SAGA or NuA4 subunits, to prevent misfolding and premature interaction with partners. Supporting this model, the ability of TTT to interact with the nascent PI3K domain of Tra1 or with Tra1 FATC mutants indicates that it can recognize both a prefolded and a misfolded form of Tra1. We speculate that TTT protects PIKKs from misfolding and degradation during translation, until ribosomes reach the end of the mRNA and produce the C-terminal FATC region, whose hydrophobicity appears essential for proper folding into a mature and stable conformation.

Evolutionary conservation of Tra1, the sole PIKK pseudokinase.

Tra1 is a member of the PIKK family but lacks catalytic residues and is thus classified as a pseudokinase. In mammals, biochemical evidence suggest a model in which the multimeric cochaperone TTT recruits the pleiotropic HSP90 chaperone to PIKKs specifically, to promote their stabilization and incorporation into active complexes. TTT binds to HSP90 indirectly, through phosphorylation-dependent interaction of TEL2 with the R2TP complex, formed by RPAP3, PIH1D1 and the AAA+ ATPases RUVBL1 and RUVBL2 (Hořejší et al., 2014, 2010; Pal et al., 2014). Surprisingly, R2TP is not conserved in *S. pombe* and Tel2 phosphorylation has no effect on PIKK stability and function (Inoue et al., 2017), although a stable TTT complex exists in *S. pombe* (Figure 1).

Despite these differences, and consistent with TTT interacting with and stabilizing *S. cerevisiae* Tra1 or human TRRAP, we demonstrate that their *S. pombe* orthologs, Tra1 and

Tra2, require Hsp90 and TTT for their incorporation into SAGA and NuA4 complexes, respectively. In agreement, we found that the TTT subunit Tti2 contributes to Tra1- and Tra2-dependent gene expression, as well as SAGA and NuA4 promoter recruitment. Therefore, although Tra1 is the sole pseudokinase within the PIKK family, it shares a dedicated chaperone machinery with active kinases for its folding, maturation, and assembly into a larger complex.

Phylogenetic analyses of PIKK orthologs in various organisms indicate that the Tra1 pseudokinase appeared early in the eukaryotic lineage, concomitantly with other PIKKs (our unpublished observations). As expected for a pseudokinase, the catalytic residues diverge substantially. However, Tra1 orthologs show high conservation of PIKK distinctive domain architecture, which consists of a long stretch of helical HEAT repeats, followed by TPR repeats forming the FAT domain, preceding FRB, PI3K-like, and FATC domains. It is thus tempting to speculate that the requirement of PIKKs for a dedicated cochaperone explains the selection pressure that is observed on the sequence and domain organization of Tra1, in the absence of conserved, functional catalytic residues. For example, the short, highly conserved C-terminal FATC domain loops back close to the active site and is critical for mTOR kinase activity (Imseng et al., 2018). Similarly, we found that the FATC is essential for Tra1 incorporation into SAGA, presumably through allosteric control of folding and positioning of the region of Tra1 that mediates its incorporation into SAGA.

Distinct architectural roles of Tra1 between the SAGA and NuA4 complexes.

Biochemical and functional evidence suggested that the Tra1 pseudokinase serves as a scaffold for the assembly and recruitment of the SAGA and NuA4 complexes to chromatin (Cheung and Díaz-Santín, 2018). *S. pombe* provides a unique opportunity to better understand its roles within each complex because it has two paralogous proteins, Tra1 and Tra2, and each has non-redundant roles that are specific for SAGA or NuA4, respectively (Helmlinger et al., 2011).

We establish that, within SAGA, Tra1 has specific regulatory roles and does not scaffold the entire complex but, rather, specifically controls the assembly of the DUB module. In contrast, Tra2 contributes to the overall architectural integrity of NuA4. In agreement, biochemical and structural analyses of yeast SAGA and NuA4 complexes reveal distinct positioning of Tra1 relative to other components. Within SAGA, Tra1 localizes to the periphery of the SAGA complex (Sharov et al., 2017) and directly interacts with Spt20 (Figure 5), whereas it occupies a more central position within NuA4 and contacts several different subunits (Wang et al., 2018). To conclude, we anticipate that, the single Tra1 protein found in most other eukaryotic organisms will have distinct structural roles between SAGA and NuA4 and function as a scaffold only for the NuA4 complex.

Topological organization of the Tra1-SAGA interface.

Additionally, in marked contrast with *S. cerevisiae* and mammals, a *tra1*Δ deletion mutant is viable in *S. pombe*, enabling detailed biochemical and genetic studies that are not possible in other organisms (Helmlinger, 2012). We indeed made significant progress in the characterization of Tra1 incorporation into SAGA. The latest structure of SAGA clearly shows that Tra1 occupies a peripheral position and interacts with the rest of the complex through a narrow and flexible surface interaction, forming a hinge (Sharov et al., 2017). Our structure-function analyses identified the residues that constitute the hinge.

Specifically, we show that a restricted, 50-residue region of the large Tra1 protein dictates the specificity of its interaction with SAGA. The homologous region from *S. pombe* Tra2 diverged such that it prevents its incorporation into SAGA. Conversely, within the hinge, an additional density predicted to form a α-helix and not attributable to Tra1 was observed at the threshold used to resolve Tra1 secondary structure elements (Sharov et al., 2017). We demonstrate that a small portion of Spt20, the HIT region, is both necessary and sufficient to anchor Tra1 within SAGA. This region of Spt20 constitutes the major interaction interface between Tra1 and the rest of SAGA, allowing the construction of unique separation-of-

function alleles for functional analyses. For example, such mutants confirmed that Tra1 of SAGA regulates the expression of a small subset of genes at steady state (Figure 6E-G).

These findings open perspectives for a better understanding of the molecular mechanism by which Tra1 modulates SAGA enzymatic activities upon binding transcription activators. Along this line, the observed structural flexibility of the hinge region might be functionally important and suggests that the interaction between Tra1 and Spt20 HIT region is highly dynamic. Understanding the molecular basis and functional relevance of this flexibility will undoubtedly be an important goal for future research projects but require novel technological approaches. Furthermore, the exact roles of Tra1/TRRAP have been challenging to study genetically because of its presence in both SAGA and NuA4 (Knutson and Hahn, 2011) and because it has essential roles in *S. cerevisiae* proliferation or during mouse early embryonic development (Herceg et al., 2001; Saleh et al., 1998). The identification of the specific residues that mediates most, if not all, Tra1-SAGA contacts enables the design of unique mutant alleles in *S. cerevisiae* and mammals for specifying the exact roles of Tra1/TRRAP within SAGA *versus* NuA4.

Ordered assembly pathway of the SAGA complex.

Biochemical analyses of SAGA in various mutants or upon Tra1 *de novo* synthesis revealed that SAGA assembly occurs through an ordered pathway, in which Spt20 recruits Tra1 which then stabilizes the incorporation of DUB subunits. Indeed, the DUB module does not affect Spt20 or Tra1 assembly and, likewise, Tra1 does not control Spt20 incorporation. However, Tra1 is presumably not directly recruiting the DUB module into SAGA. Recent structural analyses indicate that Tra1 does not stably contact any DUB component in the majority of mature SAGA complexes (Sharov et al., 2017). Rather, Tra1 might stabilize DUB incorporation during the assembly process, either through transient, direct interaction or indirectly, by inducing a conformational change within Spt20 that promotes SAGA-DUB interactions. Indeed, combining our work with previous structural and biochemical analyses

suggest that Spt20 might directly contact the DUB anchor subunit, Sgf73, although a higher resolution structure of SAGA is eventually needed to validate this hypothesis.

Overall, our findings contribute to our understanding of how multifunctional chromatin regulatory complexes are assembled, which is essential to better characterize their structural organization and functions. Tra1 mediates the trans-activation signal from promoter-bound transcription factors to SAGA and NuA4 regulatory activities, which have critical roles in both basal and inducible RNA polymerase II transcription. Our work opens exciting prospects for the characterization of SAGA and NuA4 functions during transcription.

Materials and methods

S. pombe procedures and growth conditions

Standard culture media and genetic manipulations were used, as described in (Forsburg and Rhind, 2006). Proliferation assays were performed by inoculating single colonies in either rich (YES) or minimal (EMM) media, growing cells at 32˚C to mid-log phase (~0.5 x 10^7 cells/ml), and counting their number at different time points. For longer time course, cultures were diluted to keep cells in constant exponential growth. For auxin-inducible targeted protein degradation (AID), cells were grown at 25˚C and treated with either 0.5 mM indol-3-acetic acid (IAA, I2886, Sigma) or ethanol. For CreER-loxP-mediated recombination, cells were treated with either 1 µM β-estradiol (E2758, Sigma) or DMSO alone.

Strain construction

All *S. pombe* strains used are listed in Table S2. Genetic crosses were performed by mating strains at 25˚C on SPAS medium. Strains with gene deletions, truncations, or C-terminally epitope-tagged proteins were constructed by PCR-based gene targeting of the respective open reading frame (ORF) with *kanMX6*, *natMX6 or hphMX6* cassettes, amplified from pFA6a backbone plasmids (Bahler et al., 1998; Hentges et al., 2005). For insertion of loxP sites, the same resistance cassettes were amplified from the pUG6 or pUG75 plasmids (Euroscarf #P30114, and #P30671, respectively) (Gueldener et al., 2002). Constructions of point mutations, internal deletions, or domain swaps in *spt20+* and *tra1+* were performed using a *ura4* cassette in a two-step *in vivo* site-directed mutagenesis procedure (Storici et al., 2001). Alternatively, CRISPR-Cas9-mediated genome editing was used, as described in (Zhang et al., 2018), particularly for marker-less N-terminal epitope tagging of *tra1+*. DNA fragments used for homologous recombination were generated by PCR, Gibson assembly cloning (kit E2611L, New England Biolabs), or gene synthesis. Cloning strategies and primers were designed using the online fission yeast database, PomBase (Lock et al., 2018). All primer sequences are listed in Table S3. Transformants were screened for correct

integration by PCR and, when appropriate, verified by Sanger sequencing or Western blotting. For each transformation, 2-4 individual clones were purified and analyzed.

Because the *tel2*+, *tti1*+, and *tti2*+ genes are essential for viability in *S. pombe* (Inoue et al., 2017; Shikata et al., 2007), C-terminal epitope tagging was performed in diploids, to generate heterozygous alleles. Their sporulation demonstrated that all C-terminally tagged Tel2, Tti2, or Tti2 strains grew similarly to wild-type controls in all conditions tested (data not shown). The same strategy was used to construct *tra2-AA* mutants (Figure S11).

Plasmid construction

Auxin-inducible degron (AID) tagging was performed using a plasmid, DHB137, which we constructed by inserting three HA epitopes in fusion with the three copies of the mini-AID sequence from pMK151 (Kubota et al., 2013). V5-PK tagging was performed using a plasmid, DHB123, which we constructed by inserting three V5 epitopes 5' to the hphMX6 cassette into pFA6a-hphMX6 (Euroscarf #P30438) (Hentges et al., 2005). For GST pull-down assays, a DNA fragment comprising nucleotides (nt) +925 to +1054 of the *S. pombe spt20* gene, corresponding to residues Asp282 to Ala324, was synthesized and amplified. This fragment was then subcloned into pGEX-4T2 (GE Healthcare Life Sciences), 3' and in frame to the GST coding sequence, using the Gibson assembly kit (E2611L, New England Biolabs) to generate the DHB179 plasmid.

RT-qPCR analysis

Reverse transcription and quantitative PCR analyses of cDNA were performed using RNA extracted from 50 mL of exponentially growing cells, as described in (Laboucarié et al., 2017), and according to the MIQE guidelines (Bustin et al., 2009). Briefly, total RNA was purified using hot, acidic phenol and contaminating DNA was removed by DNase I digestion, using the TURBO DNA-free™ kit (AM1907, Ambion). 1 µg of RNA was then reverse-transcribed (RT) at 55˚C with random hexanucleotide primers, using the SuperScript III First-

Strand System (18080051, ThermoFisher Scientific). Fluorescence-based quantitative PCR was performed with SYBR Green and used to calculate relative cDNA quantities, from the slope produced by standard curves for each primer pair, in each experiment. DNase-treated RNA samples were used as controls for the presence of genomic DNA contaminants. Standard curve slopes were comprised between -3.5 (90% efficiency) and -3.15 (110% efficiency), with an $r^2 > 0.9$. All primer sequences are listed in Table S3.

Protein extraction

Protein extracts were prepared as described in (Laboucarié et al., 2017). Briefly, 10 to 25 mL cultures of exponentially growing cells were homogenized by glass bead-beating in a FastPrep (MP Biomedicals). Proteins extracted using either standard lysis buffer (WEB: 40 mM HEPES-NaOH pH 7.4, 350 mM NaCl, 0.1% NP40, and 10% glycerol) or trichloroacetic acid (TCA) precipitation. WEB was supplemented with protease inhibitors, including cOmplete EDTA-free cocktails tablets (04693132001, Roche), 1 mM PMSF (P7626, Sigma), 1 μg/ml bestatin (B8385, Sigma), and 1 μg/ml pepstatin A (P5318, Sigma). Protein concentrations were measured by the Bradford method. Ponceau red or Coomassie blue staining were used to normalize for total protein levels across samples.

Western blotting and antibodies

Western blotting was performed using the following antibodies: peroxidase-anti-peroxidase (PAP) (P1291, Sigma), anti-Calmodulin binding protein (CBP) (RCBP-45A-Z, ICLab), anti-tubulin (B-5-1-2, Sigma), anti-FLAG (M2, F1804, Sigma), anti-MYC (9E10, Agro-Bio LC; 9E11, ab56, Abcam; and rabbit polyclonal ab9106, Abcam), anti-V5 (SV5-Pk1, AbD Serotec), anti-HA (16B12, Ozyme; rabbit polyclonal, ab9110, Abcam). Protein concentrations were measured by the Bradford method and used to load equal amounts of proteins across samples. Quantification of signal intensity was performed using staining, film exposure, or digital acquisition that were within the linear range of detection, as verified by

loading serial dilutions of one sample, and analyzed with Image Studio™ Lite 4.0 (LI-COR Biosciences).

Chromatin immunoprecipitation

ChIP experiments were performed as previously described (Helmlinger et al., 2011). Briefly, cell cultures were crosslinked in 1% formaldehyde for 30 min. Cells were then broken using a FastPrep (MP Biomedicals), and the chromatin fraction was sheared to 200–500 bp fragments using a Branson sonicator for 9 cycles (10 seconds ON, 50 seconds OFF) at an amplitude of 20%. For immunoprecipitation (IP), 3-5 µg of anti-HA (16B12) or anti-Myc antibodies (9E11) were incubated overnight at 4°C with the chromatin extracts and then coupled with 50 µl of protein-G-sepharose beads (GE17-0618-01, Sigma) during 4h at 4°C. ChIP DNA was quantified by fluorescence-based quantitative PCR using SYBR Green, as described for RT-qPCR analysis. Input (IN) samples were diluted 200-fold while IP samples were diluted 3-fold. Relative occupancy levels were determined by dividing the IP by the IN value (IP/IN) for each amplicon. To determine the specificity of enrichment of the tagged protein, the corresponding untagged control samples were included in each ChIP experiment. All primer sequences are listed in Table S3.

RNA immunoprecipitation

RIP experiments were done as previously described (Duncan and Mata, 2011) with minor modifications. Briefly, 100 mL of exponentially growing cells were harvested and broken using a FastPrep (MP Biomedicals). Immunoprecipitation (IP) was performed using Dynabeads® Pan-Mouse IgG (11041, ThermoFisher Scientific) that were pre-incubated with 3µg of anti-HA (16B12) or anti-MYC (9E11) antibodies overnight at 4°C. 4 mg of total protein were incubated for 2 hours at 4°C. Input (IN) and IP RNAs were extracted using the Invitrogen Purelink RNA Mini (12183018A, ThermoFisher Scientific) and Micro kits (12183016), respectively. DNase treatment, reverse transcription, and qPCR analyses of

cDNA were performed as described for RT-qPCR analysis. IN samples were diluted 50-fold while IP samples were diluted 3-to-5-fold. Relative binding levels were determined by dividing the IP by the IN value (IP/IN) for each amplicon. To determine the specificity of enrichment of the tagged protein, the corresponding untagged control samples were included in each RIP experiment. All primer sequences are listed in Table S3.

Affinity purification

Protein complexes were purified by the tandem affinity purification (TAP) method, as described previously (Helmlinger et al., 2008; Rigaut et al., 1999), with minor modifications. 1-4 liters of exponentially growing cells were harvested, snap-frozen as individual droplets, and grinded in liquid nitrogen using a Freezer/Mill® (Spex SamplePrep). Protein extraction was performed in either WEB buffer or CHAPS-containing lysis buffer (CLB) buffer (50mM HEPES-NaOH pH 7.4, 300mM NaCl, 5mM CHAPS, 0.5mM DTT), supplemented with protease and phosphatase inhibitors. Following purifications, 10% of 2 mM EGTA eluates were concentrated and separated on 4%–20% gradient SDS-polyacrylamide Tris-glycine gels (Biorad). Total protein content was visualized by silver staining, using the SilverQuest kit (LC6070, ThermoFisher Scientific). For quantitative mass spectrometry analyses, 90% of 2 mM EGTA eluates were precipitated with TCA and analyzed by mass spectrometry (MS). A downscaled version of the TAP procedure was used for standard co-immunoprecipitation followed by Western blot analysis, as described in (Laboucarié et al., 2017).

Recombinant GST and GST-HIT proteins were produced by IPTG induction of transformed BL21 Rosetta strains and purified on 100 μl of Glutathione Sepharose 4B beads (17075601, GE Healthcare Life Sciences), for 4-5 hours at 4°C. After washing, beads were further incubated overnight at 4°C with 5-10 mg of *S. pombe* protein extracts prepared in WEB lysis buffer, before analysis by Coomassie blue staining and Western blotting.

Mass spectrometry and data analysis

Dry TCA precipitates from TAP eluates were denatured, reduced and alkylated. Briefly, each sample was dissolved in 89 µL of TEAB 100 mM. One microliter of DTT 1 M was added and incubation was performed for 30 min at 60°C. A volume of 10 µL of IAA 0.5 M was added (incubation for 30 min in the dark). Enzymatic digestion was performed by addition of 1 µg trypsin (Gold, Promega, Madison USA) in TEAB 100 mM and incubation overnight at 30°C. After completing the digestion step, peptides were purified and concentrated using OMIX Tips C18 reverse-phase resin (Agilent Technologies Inc.) according to the manufacturer's specifications. Peptides were dehydrated in a vacuum centrifuge.

Samples were resuspended in 9 µL formic acid (0.1%, buffer A) and 2 µL were loaded onto a 15 cm reversed phase column (75 mm inner diameter, Acclaim Pepmap 100® C18, Thermo Fisher Scientific) and separated with an Ultimate 3000 RSLC system (Thermo Fisher Scientific) coupled to a Q Exactive Plus (Thermo Fisher Scientific) via a nano-electrospray source, using a 143-min gradient of 2 to 40% of buffer B (80% ACN, 0.1% formic acid) and a flow rate of 300 nl/min.

MS/MS analyses were performed in a data-dependent mode. Full scans (375 – 1,500 m/z) were acquired in the Orbitrap mass analyzer with a 70,000 resolution at 200 m/z. For the full scans, 3 x 106 ions were accumulated within a maximum injection time of 60 ms and detected in the Orbitrap analyzer. The twelve most intense ions with charge states ≥ 2 were sequentially isolated to a target value of 1 x 105 with a maximum injection time of 45 ms and fragmented by HCD (Higher-energy collisional dissociation) in the collision cell (normalized collision energy of 28%) and detected in the Orbitrap analyzer at 17,500 resolution.

Raw spectra were processed using the MaxQuant environment (v.1.5.5.1) (Cox and Mann, 2008) and Andromeda for database search with label-free quantification (LFQ), match between runs and the iBAQ algorithm enabled (Cox et al., 2011). The MS/MS spectra were matched against the UniProt Reference proteome (Proteome ID UP000002485) of *S. pombe*

(strain 972 / ATCC 24843) (Fission yeast) (release 2017_10; https://www.uniprot.org/) and 250 frequently observed contaminants as well as reversed sequences of all entries. Enzyme specificity was set to trypsin/P, and the search included cysteine carbamidomethylation as a fixed modification and oxidation of methionine, and acetylation (protein N-term) and/or phosphorylation of Ser, Thr, Tyr residue (STY) as variable modifications. Up to two missed cleavages were allowed for protease digestion. FDR was set at 0.01 for peptides and proteins and the minimal peptide length at 7.

The relative abundance of proteins identified in each affinity purification was calculated as described in (Smits et al., 2013). Briefly, label-free quantification (LFQ) intensity based values were transformed to a base 2 logarithmic scale (Log2), to fit the data to a Gaussian distribution and enable the imputation of missing values. Normalized LFQ intensities were compared between replicates, using a 1% permutation-based false discovery rate (FDR) in a two-tailed Student's t-test (Table S1). The threshold for significance was set to 1 (fold change = 2), based on the FDR and the ratio between TAP and 'no TAP' samples. The relative abundance of subunits in each purification eluate was obtained by dividing the LFQ intensity of that interactor (prey) to the LFQ intensity of the TAP purified protein (bait). For scaling purpose (Figure 4B and 6B,C), this ratio was further normalized to that obtained in control conditions and expressed as percentage.

RNA-seq and data analysis

All strains were done in triplicate. RNA was extracted from 50 mL of exponentially growing cells RNA using TRIzol reagent (15596018, ThermoFisher Scientific). DNA was removed by DNase I digestion, using the TURBO DNA-free™ kit (AM1907, Ambion) and RNA was cleaned using the RNeasy Mini kit (74104, Qiagen). Total RNA quality and concentration was determined using an Agilent Bioanalyzer. Transcripts were purified by polyA-tail selection. Stranded dual-indexed cDNA libraries were constructed using the Illumina TruSeq

Stranded mRNA Library Prep kit. Library size distribution and concentration were determined using an Agilent Bioanalyzer. 48 libraries were sequenced in one lane of an Illumina HiSeq 4000, with 1x 50 bp single reads, at Fasteris SA (Plan-les-Ouates, Switzerland). After demultiplexing according to their index barcode, the total number of reads ranged from 6 to 10 million per library.

Adapter sequences were trimmed from reads in the Fastq sequence files. Reads were aligned using HISAT2 (Kim et al., 2015), with strand-specific information (--rna-strandness R) and otherwise default options. For all 48 samples, the overall alignment rate was over 95%, including over 90% of reads mapping uniquely to the *S. pombe* genome. Reads were then counted for gene and exon features using htseq-count (Anders et al., 2015) in union mode (--mode union), reverse stranded (--stranded Reverse), and a minimum alignment quality of 10 (--minaqual 10). For all samples, over 95% of reads were assigned to a feature (--type gene). Variance-mean dependence was estimated from count tables and tested for differential expression based on a negative binomial distribution, using DESeq2 (Love et al., 2014). Pairwise comparison or one-way analysis of variance were run with a parametric fit and genotype as the source of variation (factor: ‘mutant’ or ‘control’). All computational analyses were run on the Galaxy web platform using the public server at usegalaxy.org (Afgan et al., 2018).

Statistical analysis

Statistical tests were performed using Graphpad Prism. *t*-tests were used when comparing two means. One-way or two-way analyses of variance (ANOVA) were performed for comparing more than two means, across one (for example “genotype”) or two distinct variables (for example “genotype” as a between-subject factors and “time” as a within-subject factor). One-way ANOVAs were followed by Tukey and two-way ANOVAs were followed by Bonferroni post-hoc pairwise comparisons. An α level of 0.01 was used *a priori*

for all statistical tests, except otherwise indicated. Comparisons that are statistically significant ($p \leq 0.01$) are marked with the star sign (*).

Data availability

The raw sequencing data reported in this paper have been deposited in the NCBI Gene Expression Omnibus under accession number ###.

Acknowledgments

We thank Kerstin Wagner and Elsa Cesari for invaluable technical assistance and all members of the Helmlinger laboratory for helpful suggestions and discussions. We are grateful to Robin Allshire, Charles Hoffman, Hisao Masukata, and Paul Russell for kindly sharing strains and to Caia Duncan and Juan Mata for assistance with RNA-IP experiments. A.E.V. is a recipient of a post-doctoral fellowship from the Fondation pour la Recherche Médicale. D.T. is a recipient of a graduate fellowship from the French Ministry for Research and Higher Education (MESR), supported by the Labex EpiGenMed, an « Investissements d'avenir » program (ANR-10-LABX-12-01). This work was supported by funds from the CNRS (ATIP-Avenir), the FP7 Marie Curie Actions (FP7-PEOPLE-2012-CIG/COACTIVATOR), and the Agence Nationale de la Recherche (ANR-15-CE12-0009-01 and ANR-15-CE11-0022-03) to D.H..

References

Afgan, E., Baker, D., Batut, B., Van Den Beek, M., Bouvier, D., Ech, M., Chilton, J., Clements, D., Coraor, N., Grüning, B.A., Guerler, A., Hillman-Jackson, J., Hiltemann, S., Jalili, V., Rasche, H., Soranzo, N., Goecks, J., Taylor, J., Nekrutenko, A., Blankenberg, D., 2018. The Galaxy platform for accessible, reproducible and collaborative biomedical analyses: 2018 update. Nucleic Acids Res. 46, W537–W544. doi:10.1093/nar/gky379

Ahmed, S., Alpi, a, Hengartner, M.O., Gartner, a, 2001. C. elegans RAD-5/CLK-2 defines a new DNA damage checkpoint protein. Curr. Biol. 11, 1934–1944. doi:S0960-9822(01)00604-2 [pii]

Alaamery, M.A., Hoffman, C.S., 2008. Schizosaccharomyces pombe Hsp90/Git10 is required for glucose/cAMP signaling. Genetics 178, 1927–1936. doi:10.1534/genetics.107.086165

Aligue, R., Akhavan-Niak, H., Russell, P., 1994. A role for Hsp90 in cell cycle control: Wee1 tyrosine kinase activity requires interaction with Hsp90. EMBO J. 13, 6099–6106.

Anders, S., Pyl, P.T., Huber, W., 2015. HTSeq-A Python framework to work with high-throughput sequencing data. Bioinformatics 31, 166–169. doi:10.1093/bioinformatics/btu638

Anderson, C.M., Korkin, D., Smith, D.L., Makovets, S., Seidel, J.J., Sali, A., Blackburn, E.H., 2008. Tel2 mediates activation and localization of ATM/Tel1 kinase to a double-strand break. Genes Dev. 22, 854–859. doi:10.1101/gad.1646208

Antonova, S. V., Haffke, M., Corradini, E., Mikuciunas, M., Low, T.Y., Signor, L., van Es, R.M., Gupta, K., Scheer, E., Vos, H.R., Tora, L., Heck, A.J.R., Timmers, H.T.M., Berger, I., 2018. Chaperonin CCT checkpoint function in basal transcription factor TFIID assembly. Nat. Struct. Mol. Biol. 25, 1119–1127. doi:10.1038/s41594-018-0156-z

Auger, A., Galarneau, L., Altaf, M., Nourani, A., Doyon, Y., Utley, R.T., Cronier, D., Allard, S., Côté, J., 2008. Eaf1 is the platform for NuA4 molecular assembly that evolutionarily

links chromatin acetylation to ATP-dependent exchange of histone H2A variants. Mol. Cell. Biol. 28, 2257–2270. doi:10.1128/mcb.01755-07

Bahler, J., Wu, J.Q., Longtine, M.S., Shah, N.G., McKenzie 3rd, A., Steever, A.B., Wach, A., Philippsen, P., Pringle, J.R., 1998. Heterologous modules for efficient and versatile PCR-based gene targeting in Schizosaccharomyces pombe. Yeast 14, 943–951. doi:10.1002/(SICI)1097-0061(199807)14:10<943::AID-YEA292>3.0.CO;2-Y

Boudreault, A.A., Cronier, D., Selleck, W., Lacoste, N., Utley, R.T., Allard, S., Savard, J., Lane, W.S., Tan, S., C??t??, J., 2003. Yeast Enhancer of Polycomb defines global Esa1-dependent acetylation of chromatin. Genes Dev. 17, 1415–1428. doi:10.1101/gad.1056603

Buchan, D.W.A., Minneci, F., Nugent, T.C.O., Bryson, K., Jones, D.T., 2013. Scalable web services for the PSIPRED Protein Analysis Workbench. Nucleic Acids Res. 41, 349–357. doi:10.1093/nar/gkt381

Bustin, S.A., Benes, V., Garson, J.A., Hellemans, J., Huggett, J., Kubista, M., Mueller, R., Nolan, T., Pfaffl, M.W., Shipley, G.L., Vandesompele, J., Wittwer, C.T., 2009. The MIQE guidelines: minimum information for publication of quantitative real-time PCR experiments. Clin. Chem. 55, 611–622. doi:10.1373/clinchem.2008.112797

Cheung, A.C.M., Díaz-Santín, L.M., 2018. Share and share alike: the role of Tra1 from the SAGA and NuA4 coactivator complexes. Transcription 00, 1–7. doi:10.1080/21541264.2018.1530936

Cox, J., Mann, M., 2008. MaxQuant enables high peptide identification rates, individualized p.p.b.-range mass accuracies and proteome-wide protein quantification. Nat. Biotechnol. 26, 1367–1372. doi:10.1038/nbt.1511

Cox, J., Neuhauser, N., Michalski, A., Scheltema, R.A., Olsen, J. V, Mann, M., 2011. Andromeda: a peptide search engine integrated into the MaxQuant environment. J. Proteome Res. 10, 1794–1805. doi:10.1021/pr101065j

Duncan, C.D., Mata, J., 2014. Cotranslational protein-RNA associations predict protein-protein interactions. BMC Genomics 15, 298. doi:10.1186/1471-2164-15-298

Duncan, C.D., Mata, J., 2011. Widespread cotranslational formation of protein complexes. PLoS Genet. 7, e1002398. doi:10.1371/journal.pgen.1002398

Forsburg, S.L., Rhind, N., 2006. Basic methods for fission yeast. Yeast 23, 173–183. doi:10.1002/yea.1347

Genereaux, J., Kvas, S., Dobransky, D., Karagiannis, J., Gloor, G.B., Brandl, C.J., 2012. Genetic evidence links the ASTRA protein chaperone component Tti2 to the SAGA transcription factor Tra1. Genetics 191, 765–780. doi:10.1534/genetics.112.140459

Goto, G.H., Ogi, H., Biswas, H., Ghosh, A., Tanaka, S., Sugimoto, K., 2017. Two separate pathways regulate protein stability of ATM/ATR-related protein kinases Mec1 and Tel1 in budding yeast. PLoS Genet. 13, 1–22. doi:10.1371/journal.pgen.1006873

Gueldener, U., Heinisch, J., Koehler, G.J., Voss, D., Hegemann, J.H., 2002. A second set of loxP marker cassettes for Cre-mediated multiple gene knockouts in budding yeast. Nucleic Acids Res. 30, e23. doi:10.1093/nar/30.6.e23

Halbach, A., Zhang, H., Wengi, A., Jablonska, Z., Gruber, I.M., Halbeisen, R.E., Dehé, P.-M.M., Kemmeren, P., Holstege, F., Géli, V., Gerber, A.P., Dichtl, B., 2009. Cotranslational assembly of the yeast SET1C histone methyltransferase complex. EMBO J. 28, 2959–2970. doi:10.1038/emboj.2009.240

Han, Y., Luo, J., Ranish, J., Hahn, S., 2014. Architecture of the Saccharomyces cerevisiae SAGA transcription coactivator complex. EMBO J. 33, 2534–46. doi:10.15252/embj.201488638

Hayashi, T., Hatanaka, M., Nagao, K., Nakaseko, Y., Kanoh, J., Kokubu, A., Ebe, M., Yanagida, M., 2007. Rapamycin sensitivity of the Schizosaccharomyces pombe tor2 mutant and organization of two highly phosphorylated TOR complexes by specific and common subunits. Genes to cells 12, 1357–1370. doi:10.1111/j.1365-2443.2007.01141.x

Helmlinger, D., 2012. New insights into the SAGA complex from studies of the Tra1 subunit in budding and fission yeast. Transcription 3, 13–18. doi:10.4161/trns.3.1.19271

Helmlinger, D., Marguerat, S., Villén, J., Gygi, S.P., Bähler, J., Winston, F., 2008. The S.

pombe SAGA complex controls the switch from proliferation to sexual differentiation through the opposing roles of its subunits Gcn5 and Spt8. Genes Dev. 22, 3184–95. doi:10.1101/gad.1719908

Helmlinger, D., Marguerat, S., Villén, J., Swaney, D.L., Gygi, S.P., Bähler, J., Winston, F., Villen, J., Swaney, D.L., Gygi, S.P., Baehler, J., Winston, F., 2011. Tra1 has specific regulatory roles, rather than global functions, within the SAGA co-activator complex. EMBO J. 30, 2843–2852. doi:10.1038/emboj.2011.181

Helmlinger, D., Tora, L., 2017. Sharing the SAGA. Trends Biochem. Sci. 42, 850–861. doi:10.1016/j.tibs.2017.09.001

Hentges, P., Van Driessche, B., Tafforeau, L., Vandenhaute, J., Carr, A.M., 2005. Three novel antibiotic marker cassettes for gene disruption and marker switching in Schizosaccharomyces pombe. Yeast 22, 1013–1019. doi:10.1002/yea.1291

Herceg, Z., Hulla, W., Gell, D., Cuenin, C., Lleonart, M., Jackson, S., Wang, Z.Q., 2001. Disruption of Trrap causes early embryonic lethality and defects in cell cycle progression. Nat. Genet. 29, 206–211. doi:10.1038/ng725

Hoffman, K.S., Duennwald, M.L., Karagiannis, J., Genereaux, J., Alexander, S., Brandl, C.J., 2016. Saccharomyces cerevisiae Tti2 regulates PIKK proteins and stress response. G3 (Bethesda). 6, 1649–1659. doi:10.1534/g3.116.029520

Hořejší, Z., Stach, L., Flower, T.G., Joshi, D., Flynn, H., Skehel, J.M., O'Reilly, N.J., Ogrodowicz, R.W., Smerdon, S.J., Boulton, S.J., 2014. Phosphorylation-dependent PIH1D1 interactions define substrate specificity of the R2TP cochaperone complex. Cell Rep. 7, 19–26. doi:10.1016/j.celrep.2014.03.013

Hořejší, Z., Takai, H., Adelman, C.A., Collis, S.J., Flynn, H., Maslen, S., Skehel, J.M., de Lange, T., Boulton, S.J., Horejsi, Z., Takai, H., Adelman, C.A., Collis, S.J., Flynn, H., Maslen, S., Skehel, J.M., de Lange, T., Boulton, S.J., Hořejší, Z., Takai, H., Adelman, C.A., Collis, S.J., Flynn, H., Maslen, S., Skehel, J.M., de Lange, T., Boulton, S.J., 2010. CK2 phospho-dependent binding of R2TP complex to TEL2 is essential for mTOR and SMG1 stability. Mol. Cell 39, 839–850. doi:10.1016/j.molcel.2010.08.037

Hurov, K.E., Cotta-Ramusino, C., Elledge, S.J., 2010. A genetic screen identifies the Triple T complex required for DNA damage signaling and ATM and ATR stability. Genes Dev. 24, 1939–1950. doi:10.1101/gad.1934210

Imseng, S., Aylett, C.H., Maier, T., 2018. Architecture and activation of phosphatidylinositol 3-kinase related kinases. Curr. Opin. Struct. Biol. 49, 177–189. doi:10.1016/j.sbi.2018.03.010

Inoue, H., Sugimoto, S., Takeshita, Y., Takeuchi, M., Hatanaka, M., Nagao, K., Hayashi, T., Kokubu, A., Yanagida, M., Kanoh, J., 2017. CK2 phospho-independent assembly of the Tel2-associated stress-signaling complexes in Schizosaccharomyces pombe. Genes to Cells 22, 59–70. doi:10.1111/gtc.12454

Izumi, N., Yamashita, A., Hirano, H., Ohno, S., 2012. Heat shock protein 90 regulates phosphatidylinositol 3-kinase-related protein kinase family proteins together with the RUVBL1/2 and Tel2-containing co-factor complex. Cancer Sci. 103, 50–57. doi:10.1111/j.1349-7006.2011.02112.x

Kaizuka, T., Hara, T., Oshiro, N., Kikkawa, U., Yonezawa, K., Takehana, K., Iemura, S.-I., Natsume, T., Mizushima, N., 2010. Tti1 and Tel2 are critical factors in mammalian target of rapamycin complex assembly. J. Biol. Chem. 285, 20109–20116. doi:10.1074/jbc.M110.121699

Kamenova, I., Mukherjee, P., Conic, S., Mueller, F., El-Saafin, F., Bardot, P., Garnier, J.-M., Dembele, D., Capponi, S., Timmers, M.H., Vincent, S.D., Tora, L., 2018. Co-translation drives the assembly of mammalian nuclear multisubunit complexes. bioRxiv 419812. doi:10.1101/419812

Kassem, S., Villanyi, Z., Collart, M.A., 2017. Not5-dependent co-translational assembly of Ada2 and Spt20 is essential for functional integrity of SAGA. Nucleic Acids Res. 45, 1186–1199. doi:10.1093/nar/gkw1059

Kim, D., Langmead, B., Salzberg, S.L., 2015. HISAT: A fast spliced aligner with low memory requirements. Nat. Methods 12, 357–360. doi:10.1038/nmeth.3317

Kim, S.G., Hoffman, G.R., Poulogiannis, G., Buel, G.R., Jang, Y.J., Lee, K.W., Kim, B.-Y.Y.,

Erikson, R.L., Cantley, L.C., Choo, A.Y., Blenis, J., 2012. Metabolic Stress Controls mTORC1 Lysosomal Localization and Dimerization by Regulating the TTT-RUVBL1/2 Complex. Mol. Cell. doi:10.1016/j.molcel.2012.10.003

Knutson, B.A., Hahn, S., 2011. Domains of Tra1 important for activator recruitment and transcription coactivator functions of SAGA and NuA4 complexes. Mol. Cell. Biol. 31, 818–831. doi:10.1128/mcb.00687-10

Köhler, A., Schneider, M., Cabal, G.G., Nehrbass, U., Hurt, E., 2008. Yeast Ataxin-7 links histone deubiquitination with gene gating and mRNA export. Nat. Cell Biol. 10, 707–715. doi:10.1038/ncb1733

Koutelou, E., Hirsch, C.L., Dent, S.Y., 2010. Multiple faces of the SAGA complex. Curr. Opin. Cell Biol. 22, 374–382. doi:10.1016/j.ceb.2010.03.005

Kubota, T., Nishimura, K., Kanemaki, M.T., Donaldson, A.D., 2013. The Elg1 Replication Factor C-like Complex Functions in PCNA Unloading during DNA Replication. Mol. Cell 50, 273–280. doi:10.1016/j.molcel.2013.02.012

Laboucarié, T., Detilleux, D., Rodriguez-Mias, R.A., Faux, C., Romeo, Y., Franz-Wachtel, M., Krug, K., Maček, B., Villén, J., Petersen, J., Helmlinger, D., 2017. TORC1 and TORC2 converge to regulate the SAGA co-activator in response to nutrient availability. EMBO Rep. 16, 202–212. doi:10.15252/embr.201744942

Lee, K.K., Sardiu, M.E., Swanson, S.K., Gilmore, J.M., Torok, M., Grant, P.A., Florens, L., Workman, J.L., Washburn, M.P., 2011. Combinatorial depletion analysis to assemble the network architecture of the SAGA and ADA chromatin remodeling complexes. Mol. Syst. Biol. 7, 503. doi:10.1038/msb.2011.40

Lempiäinen, H., Halazonetis, T.D., 2009. Emerging common themes in regulation of PIKKs and PI3Ks. EMBO J. 28, 3067–3073. doi:10.1038/emboj.2009.281

Lock, A., Rutherford, K., Harris, M.A., Hayles, J., Oliver, S.G., Bähler, J., Wood, V., 2018. PomBase 2018: user-driven reimplementation of the fission yeast database provides rapid and intuitive access to diverse, interconnected information. Nucleic Acids Res. 1–7. doi:10.1093/nar/gky961

Love, M.I., Huber, W., Anders, S., 2014. Moderated estimation of fold change and dispersion for RNA-seq data with DESeq2. Genome Biol. 15, 1–21. doi:10.1186/s13059-014-0550-8

Lu, P.Y.T., Lévesque, N., Kobor, M.S., 2009. NuA4 and SWR1-C: two chromatin-modifying complexes with overlapping functions and components. Biochem. Cell Biol. 87, 799–815. doi:10.1139/O09-062

Marsh, J.A., Teichmann, S.A., 2015. Structure, Dynamics, Assembly, and Evolution of Protein Complexes. Annu. Rev. Biochem. 84, 551–575. doi:10.1146/annurev-biochem-060614-034142

McMahon, S.B., Van Buskirk, H.A., Dugan, K.A., Copeland, T.D., Cole, M.D., 1998. The novel ATM-related protein TRRAP is an essential cofactor for the c-Myc and E2F oncoproteins. Cell 94, 363–374.

Nagy, Z., Riss, A., Romier, C., le Guezennec, X., Dongre, A.R., Orpinell, M., Han, J., Stunnenberg, H., Tora, L., 2009. The Human SPT20-Containing SAGA Complex Plays a Direct Role in the Regulation of Endoplasmic Reticulum Stress-Induced Genes. Mol. Cell. Biol. 29, 1649–1660. doi:10.1128/MCB.01076-08

Pal, M., Morgan, M., Phelps, S.E.L., Roe, S.M., Parry-Morris, S., Downs, J.A., Polier, S., Pearl, L.H., Prodromou, C., 2014. Structural basis for phosphorylation-dependent recruitment of Tel2 to Hsp90 by Pih1. Structure 22, 805–818. doi:10.1016/j.str.2014.04.001

Rigaut, G., Shevchenko, A., Rutz, B., Wilm, M., Mann, M., Seraphin, B., 1999. A generic protein purification method for protein complex characterization and proteome exploration. Nat. Biotechnol. 17, 1030–1032. doi:10.1038/13732

Rozario, D., Siede, W., 2012. Saccharomyces cerevisiae Tel2 plays roles in TORC signaling and telomere maintenance that can be mutationally separated. Biochem. Biophys. Res. Commun. 417, 1182–1187. doi:10.1016/j.bbrc.2011.12.103

Saleh, A., Schieltz, D., Ting, N., McMahon, S.B., Litchfield, D.W., Yates, J.R., Lees-Miller, S.P., Cole, M.D., Brandl, C.J., 1998. Tra1p is a component of the yeast Ada·Spt

transcriptional regulatory complexes. J. Biol. Chem. 273, 26559–26565. doi:10.1074/jbc.273.41.26559

Setiaputra, D., Ross, J.D., Lu, S., Cheng, D.T., Dong, M.Q., Yip, C.K., 2015. Conformational flexibility and subunit arrangement of the modular yeast Spt-Ada-Gcn5 acetyltransferase complex. J. Biol. Chem. 290, 10057–10070. doi:10.1074/jbc.M114.624684

Sharov, G., Voltz, K., Durand, A., Kolesnikova, O., Papai, G., Myasnikov, A.G., Dejaegere, A., Shem, A. Ben, Schultz, P., 2017. Structure of the transcription activator target Tra1 within the chromatin modifying complex SAGA. Nat. Commun. 8, 1556. doi:10.1038/s41467-017-01564-7

Shevchenko, A.A., Roguev, A., Schaft, D., Buchanan, L., Habermann, B., Sakalar, C., Thomas, H., Krogan, N.J., Shevchenko, A.A., Stewart, A.F., 2008. Chromatin Central: towards the comparative proteome by accurate mapping of the yeast proteomic environment. Genome Biol. 9, R167. doi:10.1186/gb-2008-9-11-r167

Shiber, A., Döring, K., Friedrich, U., Klann, K., Merker, D., Zedan, M., Tippmann, F., Kramer, G., Bukau, B., 2018. Cotranslational assembly of protein complexes in eukaryotes revealed by ribosome profiling. Nature 561, 268–272. doi:10.1038/s41586-018-0462-y

Shieh, Y.W., Minguez, P., Bork, P., Auburger, J.J., Guilbride, D.L., Kramer, G., Bukau, B., 2015. Operon structure and cotranslational subunit association direct protein assembly in bacteria. Science (80-.). 350, 678–680. doi:10.1126/science.aac8171

Shikata, M., Ishikawa, F., Kanoh, J., 2007. Tel2 is required for activation of the Mrc1-mediated replication checkpoint. J. Biol. Chem. 282, 5346–5355. doi:10.1074/jbc.M607432200

Smits, A.H., Jansen, P.W.T.C., Poser, I., Hyman, A.A., Vermeulen, M., 2013. Stoichiometry of chromatin-associated protein complexes revealed by label-free quantitative mass spectrometry-based proteomics. Nucleic Acids Res. 41, e28. doi:10.1093/nar/gks941

Spedale, G., Timmers, H.T., Pijnappel, W.W., 2012. ATAC-king the complexity of SAGA during evolution. Genes Dev. 26, 527–541. doi:10.1101/gad.184705.111

Stirling, P.C., Bloom, M.S., Solanki-Patil, T., Smith, S., Sipahimalani, P., Li, Z., Kofoed, M., Ben-Aroya, S., Myung, K., Hieter, P., 2011. The complete spectrum of yeast chromosome instability genes identifies candidate CIN cancer genes and functional roles for ASTRA complex components. PLoS Genet. 7. doi:10.1371/journal.pgen.1002057

Storici, F., Lewis, L.K., Resnick, M.A., 2001. In vivo site-directed mutagenesis using oligonucleotides. Nat. Biotechnol. 19, 773–776. doi:10.1038/90837

Takai, H., Wang, R.C., Takai, K.K., Yang, H., de Lange, T., 2007. Tel2 Regulates the Stability of PI3K-Related Protein Kinases. Cell 131, 1248–1259. doi:10.1016/j.cell.2007.10.052

Takai, H., Xie, Y., de Lange, T., Pavletich, N.P., 2010. Tel2 structure and function in the Hsp90-dependent maturation of mTOR and ATR complexes. Genes Dev. 24, 2019–2030. doi:10.1101/gad.1956410

Vassilev, A., Yamauchi, J., Kotani, T., Prives, C., Avantaggiati, M.L., Qin, J., Nakatani, Y., 1998. The 400 kDa subunit of the PCAF histone acetylase complex belongs to the ATM superfamily. Mol. Cell 2, 869–875.

Wang, X., Ahmad, S., Zhang, Z., Côté, J., Cai, G., 2018. Architecture of the Saccharomyces cerevisiae NuA4/TIP60 complex. Nat. Commun. 9, 1147. doi:10.1038/s41467-018-03504-5

Wu, P.-Y.J.Y., Winston, F., 2002. Analysis of Spt7 function in the Saccharomyces cerevisiae SAGA coactivator complex. Mol. Cell. Biol. 22, 5367–5379. doi:10.1128/MCB.22.15.5367-5379.2002

Zhang, X.-R., He, J.-B., Wang, Y.-Z., Du, L.-L., 2018. A Cloning-Free Method for CRISPR/Cas9-Mediated Genome Editing in Fission Yeast. G3 (Bethesda). 8, g3.200164.2018. doi:10.1534/g3.118.200164

Figure Legends

Figure 1. The Tti2 subunit of the TTT complex contributes to Tra1 and Tra2 functions in gene expression.

(A) Mass spectrometry analysis (LC-MS/MS) of tandem affinity purified Tti2 (Tti2-TAP = bait). Volcano plot showing the average ratios of label-free quantification (LFQ) intensities in Tti2-TAP over control 'no TAP' purifications by normalized *P* values (*q*), computed from four independent experiments. Each dot represents one protein, with known TTT subunits coloured in orange and Tti2-interacting proteins in green. Rvb1, which dimerizes with Rvb2, is shown in light orange because of weak reproducibility of its binding across experiments.

(B) Schematic depiction of TTT complex components (orange) and their interacting PIKK clients (light green), shown within their complexes (dark green). *S. pombe* protein name abbreviations are shown, with their human orthologs in superscript.

(C) Hierarchical clustering analysis of the transcriptome profiles of control *cre-ER* (*cre* (WT)), inducible *tti2+* (*tti2-CKO*) and *tra2+* knock-outs (*tra2-CKO*), and *tra1*Δ mutants (columns). Differential gene expression analysis was performed comparing cells treated with either DMSO (control) or β-estradiol (KO) for 21 hours (h) (*cre-ER* and *tra2-CKO* strains) or 18 h (*tti2-CKO* strain). *tra1*Δ mutants were compared to isogenic wild-type (WT) control cells. Rows represent genes that are differentially expressed in at least one condition ($P \leq 0.01$) and clustered based on Pearson distance. The Log2 of their fold-change in each condition is colour coded, as indicated.

(D) Venn diagrams showing the overlap between genes that are differentially expressed (FC ≥ 1.5, $P \leq 0.01$) in inducible *tti2-CKO* (n = 184), *tra2-CKO* (n = 153), and *tra1*Δ mutants (n = 59). Genes which expression is β-estradiol-regulated (see Figure S4A) have been filtered out before constructing the diagrams.

(E) SAGA and NuA4 promoter binding upon inducible *tti2* knock-out. Chromatin immunoprecipitation followed by quantitative PCR (ChIP-qPCR) analysis was performed using *tti2-CKO* cells treated with either DMSO (+) or β-estradiol (-) for 18 h. ChIP of Spt7-MYC at the *pho84+* and *mei2+* promoters or of Epl1-MYC at the *ssa2+* promoter serve as proxies for SAGA or NuA4 binding, respectively. A non-tagged strain was used as control for background IP signal (MYC: no). Ratios of MYC ChIP to input (IP/IN) from three independent experiments are shown as individual points, overlaid with the mean and SEM. Statistical significance was determined by one-way ANOVA followed by Tukey's multiple comparison tests (*$P < 0.05$).

(F) Anti-MYC and –HA Western blotting of Tti2-HA, Spt7-MYC, and Epl1-MYC in the input fraction of the chromatin samples used for the ChIP-qPCR experiments shown in (E). Equal loading was controlled using an anti-tubulin antibody.

Figure 2: Tti2 promotes the incorporation of Tra1/Tra2 into SAGA/NuA4 complexes.

(A) Silver staining of SAGA complexes purified either in the presence or absence of Tti2 (left). *spt7-TAP tti2-CKO* cells were grown to exponential phase in rich medium supplemented with either DMSO (+Tti2) or β-estradiol (-Tti2) for 18 h. SAGA was purified from a *tra1*Δ strain as a control for the complete loss of Tra1 from SAGA. LC-MS/MS analyses of SAGA purifications (right). LFQ intensity ratios of Tra1 to the bait, Spt7, from two biological replicates are plotted individually with the mean (black bar). Below are anti-HA Western blotting of Spt7-TAP and Tti2-HA in a fraction of the input used for TAP.

(B) Silver staining of NuA4 complexes purified either in presence or absence of Tti2 (left). *mst1-TAP tti2-CKO* cells were grown to exponential phase in rich medium supplemented with either DMSO (+Tti2) or β-estradiol (-Tti2) for 18 h. LC-MS/MS analyses of NuA4 purifications (right). LFQ intensity ratios of Tra2 to the bait, Mst1, from two biological replicates are plotted individually with the mean (black bar). Below are anti-HA Western blotting of Mst1-TAP and Tti2-HA in a fraction of the input used for TAP.

(C) Silver staining of SAGA complexes purified upon Tra1 *de novo* expression, either in presence or absence of Tel2. *spt7-TAP RI-tra1 tel2-AID* cells were grown to exponential phase in rich medium, supplemented with either ethanol (-IAA) or auxin (+IAA) for 16 h, and harvested 6 hours after addition of either DMSO (-) or β-estradiol (+). SAGA was purified from an untreated WT strain as a positive control. Numbers at the bottom of the gel represent LFQ intensity ratios of Tra1 to the bait, Spt7, from LC-MS/MS analyses of purified SAGA complexes (N.A.: not analyzed). Below are anti-HA Western blotting of Spt7-TAP and Tel2-AID in a fraction of the input used for TAP. Both the TAP and AID sequences are in frame with HA epitopes. Ponceau red staining is used as loading control. Shown are data that are representative of two independent experiments.

(D) Silver staining of SAGA complexes purified upon Tra1 *de novo* expression, in WT and *hsp90-201* mutant strains. *spt7-TAP RI-tra1 hsp90+* and *spt7-TAP RI-tra1 hsp90-201* cells were grown to exponential phase in rich medium and harvested 6 hours after addition of either DMSO (-) or β-estradiol (+). Numbers at the bottom of the gel represent LFQ intensity ratios of Tra1 to the bait, Spt7, from LC-MS/MS analyses of purified SAGA complexes. Below are anti-HA Western blotting of Spt7-TAP in a fraction of the input used for TAP. Ponceau red staining is used as loading control. Shown are data that are representative of two independent experiments.

(E) Silver staining of NuA4 complexes purified either in presence or absence of Tra2, using Epl1-TAP (left) or Vid21-TAP (right) as baits. *epl1-TAP tra2-CKO* and *vid21-TAP tra2-CKO*

cells were grown to exponential phase in rich medium supplemented with either DMSO (+Tra2) or β-estradiol (-Tra2).

(F) A scatter plot representing the LFQ intensities from LC-MS/MS analysis of NuA4 complexes purified in the presence (x-axis) or absence (y-axis) of Tra2. Individual points represent individual NuA4 subunits in Vid21-TAP eluates. The dashed line shows a 1:1 ratio.

Figure 3: The TTT complex binds *tra1*+ and *tra2*+ mRNAs co-translationally.

(A) The TTT component Tel2 is not enriched at Spt7-bound promoters. ChIP-qPCR analysis of Tel2 occupancy at the *ssa2*+ and *mei2*+ promoters, as compared to Spt7. A non-tagged strain was used as control for background IP signal (no HA). Ratios of HA ChIP to input (IP/IN) from three independent experiments are shown as individual points, overlaid with the mean and SEM.

(B-F) RNA immunoprecipitation followed by qPCR experiments (RIP-qPCR). HA (B-D) or MYC (E,F) IPs were performed using RNA extracted from cells grown to exponential phase. Ratios of IP to input (IP/IN) from independent experiments are shown as individual points, overlaid with the mean and SD. (B-E) The *isp6*+ mRNA is used as negative control. A non-tagged strain (B,E,F) and a strain with a tag fused to a protein not interacting with TTT, Ste20 (B,D), were used as controls for background IP signal. The red-coloured dashed line indicates unspecific background signal within each experiment.
(B) RT-PCR (top) and –qPCR (bottom) analyses of *tra1*+ mRNA binding to TTT subunits.
(C) RIP-qPCR analysis of *tra1*+, *tra2*+ exon, and *tra2*+ intron mRNAs in Tti1-HA IPs from control, puromycin-, or EDTA-treated samples.
(D) RIP-qPCR analysis of *tra1*+, *ada1*+, *taf12*+, and *spt20*+ mRNAs in Tel2-HA IPs.
(E) RIP-qPCR analysis of *tra2*+, *vid21*+, *epl1*+, and *eaf7*+ mRNAs in Tti2-MYC IPs.
(F) RIP-qPCR analysis of *tra1*+ and *tra2*+ mRNAs in Tti2-MYC, Spt20-MYC, and Epl1-MYC IPs.

Figure 4: Structure-function analysis of Tra1 interaction with SAGA and TTT.

(A) Schematic illustration of C-terminal truncation and point mutant alleles of *S. pombe tra1+*. Distinct colours depict Tra1 domains: HEAT, FAT, PI3K, and FATC. Truncation mutations remove the FATC (*tra1-1*), the PI3K and the FATC (*tra1-2*), half of the FAT, PI3K and FATC (*tra1-3*), or the entire FAT, PI3K and FATC domains (*tra1-4*). The last residue of each truncated mutant protein is shown. The *tra1-AA* allele was constructed by substituting the last two hydrophobic amino-acids with alanine residues.

(B) Silver staining of SAGA complexes purified from a WT strain and different *tra1* mutants, using Spt7 as the bait. A non-tagged strain (no TAP) was used as a control for background. Numbers at the bottom of the gel represent LFQ intensity ratios of Tra1 to Spt7, from LC-MS/MS analyses of purified SAGA complexes. Values for each mutant are expressed as percentage of WT SAGA. Shown are gels that are representative of three independent experiments.

(C-D) Mutation of Tra1 FATC domain recapitulates the HU sensitivity (C) and gene expression changes (D) observed in *tra1*Δ mutants. (C) HU sensitivity was assessed by spotting ten-fold serial dilutions of exponentially growing cells of the indicated genotypes either on rich medium (control), or medium supplemented with 10 mM HU, and incubated for 3 days at 32°C. (D) A scatter plot from RNA-seq count data comparing *tra1*Δ mutants (x-axis) with *tra1-AA* mutants (y-axis), relative to isogenic WT controls. Statistical significance and correlation were analyzed by computing the Pearson correlation coefficient ($r^2 = 0.75$, $P < 0.001$). The black dashed line represents a 1:1 ratio.

(E) LC-MS/MS analysis of TTT complexes purified from a WT strain and different *tra1* mutants, using Tti2 as the bait. LFQ intensity ratios of Tra1 to Tti2 from 2-4 biological replicates are plotted individually with the mean (black bar).

(F) RIP-qPCR analysis of *tra1+* and *isp6+* mRNAs in Tti2-HA IPs from a WT strain and *tra1-2* and *tra1-4* truncation mutants. The red-coloured dashed line indicates unspecific background signal, defined by the maximal amount of *isp6+* mRNA recovered. A non-tagged strain was used as a negative control.

(G) Cycloheximide (CHX) chase analysis of Tra1 stability. Anti-FLAG Western blotting of extracts from WT (*tra1+*) and *tra1-AA* mutant strains grown to exponential phase in rich medium and treated with CHX for 0, 3 and 6 hours. An anti-Rbp1 antibody served as loading control. Shown are blots that are representative of three independent experiments.

Figure 5: Identification of the specific SAGA-interacting region of Tra1.

(A) Close-up view of the putative region of Tra1 that contacts the rest of SAGA, which constitutes the flexible hinge in the structure of *Pichia pastoris* SAGA (EMD: 3804). Cartoon cylinders represent α-helices in *P. Pastoris* Tra1 structure (PDB: 5OEJ). This domain is located near the start of the FAT domain and corresponds to residues 2700-2753 (brown-coloured box). A homologous region, defined as the Cup SAGA Interacting (CSI), was identified in *S. pombe* Tra1 (residues 2623-2676) from multiple alignments of Tra1 orthologs, shown at the bottom. Residues that appear unique to *S. pombe* Tra2 are underlined (green).

(B) Schematic illustration of the hybrid mutant alleles of *S. pombe tra1*+ that were constructed. Residues 2623-2676 from *S. pombe* Tra1 were swapped with the homologous region from either *S. pombe* Tra2 (green, residues 2564-2617), to create the *tra1-Sptra2* allele, or *S. cerevisiae* Tra1 (blue, residues 2698-2751), to create the *tra1-Sctra1* allele.

(C) Silver staining of SAGA complexes purified from WT, *tra1-Sptra2*, and *tra1-Sctra1* strains (see B), using Spt7 as the bait. A non-tagged strain (no TAP) was used as a control for background. Numbers at the bottom of the gel represent LFQ intensity ratios of Tra1 to the bait, Spt7, from LC-MS/MS analyses of purified SAGA complexes (ND: not detected). Below are anti-FLAG and anti-HA Western blotting of FLAG-Tra1 and Spt7-TAP in a fraction of the input used for TAP. Shown are gels that are representative of five independent experiments.

(D-E) HU sensitivity (D) and gene expression changes (E,F) of *tra1-Sptra2*, *tra1-Sctra1*, as compared to *tra1*Δ mutants. (D) Ten-fold serial dilutions of exponentially growing cells of the indicated genotypes were spotted on rich medium (control), medium supplemented with 10 mM HU, or 15 mM caffeine, and incubated at 32°C. (E,F) Scatter plots from RNA-seq count data comparing *tra1*Δ mutants (x-axis) with either *tra1-Sptra2* mutants (y-axis in E) or *tra1-Sctra1* mutants (y-axis in F), relative to isogenic WT controls. Statistical significance and correlation were analyzed by computing the Pearson correlation coefficient (r^2 = 0.58 for *tra1-Sptra2 vs*. *tra1*Δ and r^2 = 0.16 for *tra1-Sctra1* vs. *tra1*Δ; $P < 0.001$). The black dashed line represents a 1:1 ratio.

Figure 6: A restricted domain of Spt20 is both necessary and sufficient to anchor Tra1 to the SAGA complex.

(A) Silver staining of SAGA complexes purified from WT and *spt20*Δ strains, using Spt7 as the bait. A band corresponding to Spt20 disappears in *spt20*Δ mutants.

(B) Schematic illustration of the different Spt20 truncation mutant alleles constructed to identify the Head Interacting with Tra1 (HIT) region of Spt20. Distinct colours depict Spt20 domains, defined as Homology Boxes (HB) and a Low Complexity Region (LCR). Each allele is named after to the last residue present in the truncation mutant, which shortens the LCR to various extent, as illustrated. Silver staining of SAGA complexes purified from WT and *spt20* truncation mutants, using Spt7 as the bait. Numbers at the bottom of the gel represent LFQ intensity ratios of Tra1 to Spt7, from LC-MS/MS analyses of SAGA purifications. Values for each mutant are expressed as percentage of WT SAGA. Purple colouring depicts the region of Spt20 that allows SAGA to interact with Tra1 in each truncation mutant.

(C) Schematic illustration of the deletion or point mutations within Spt20 HIT region, narrowed down to residues 290-300 (purple-coloured box) and predicted to fold into a α-helix, using PSI-blast based secondary structure PREDiction (PSIPRED, (Buchan et al., 2013)). Silver staining of SAGA complexes purified from WT, *spt20-HIT*Δ, s*pt20-FIEN*, and *spt20-RRKR* mutants, using Spt7 as the bait. Numbers at the bottom of the gel represent LFQ intensity ratios of Tra1 to Spt7, from LC-MS/MS analyses of purified SAGA complexes. Values for each mutant are expressed as percentage of WT SAGA. (B,C) Asterisks indicate the position of the WT and mutant Spt20 proteins in purified SAGA.

(D-G) HU sensitivity of *spt20-HIT*Δ, s*pt20-FIEN*, and *spt20-RRKR* mutants, as compared to *tra1*Δ mutant strains. Ten-fold serial dilutions of exponentially growing cells of the indicated genotypes were spotted either on rich medium (control) or medium supplemented with 5 mM HU and incubated for 3 days at 32°C.

(E-G) Scatter plots from RNA-seq data comparing *spt20-HITD*Δ mutants (y-axis) with either *spt20*Δ mutants (x-axis in E), *tra1*Δ mutants (x-axis in F), or *tra1-Sptra2* mutants (x-axis in G), relative to isogenic WT controls. Statistical significance and correlation were analyzed by computing the Pearson correlation coefficient (r^2 = 0.35 for *spt20-HIT*Δ *vs. spt20*Δ; r^2 = 0.44 for *spt20-HIT*Δ *vs*. *tra1*Δ; r^2 = 0.62 for *spt20-HIT*Δ *vs. tra1-Sptra2*; $P < 0.001$). The black dashed line represents a 1:1 ratio.

(H) GST pull-down of *S. pombe* protein extracts from WT, *tra1-Sptra2*, and *tra1-Sctra1* strains, using GST alone or GST fused to Spt20 HIT region (residues 282-325). Coomassie

blue staining of purified GST fusion proteins (left panel). Anti-FLAG Western blotting of WT and hybrid Tra1 proteins bound to GST or GST-HIT columns (right panel) and of a fraction (0.6%) of the input used for the pull-downs. Shown are gels that are representative of three independent experiments.

Figure 7: Tra1 promotes the incorporation of the DUB module within SAGA.

(A,B) LC-MS/MS analysis of SAGA complexes purified from mutants defective in Tra1-SAGA interaction, including *tra1*Δ (n = 2) and β-estradiol treated *tti2-CKO* mutants (-Tti2, n = 2), as well as four distinct mutant alleles that disrupt the hinge region (Hinge*). These include *tra1-Sptra2*, *spt20-290*, *spt20-HIT*Δ, and *spt20-FIEN* mutants, labelled from dark to light green, respectively. Relative LFQ intensity ratios of Sgf73 (A) and Ubp8 (B) to the bait, Spt7, from independent experiments or mutants are plotted individually.

(C) Silver staining of SAGA complexes purified from WT (*sgf73*+) or *sgf73*Δ mutants, using Ada1 as the bait. Shown are gels that are representative of three independent experiments.

(D) Silver staining and Western blotting of SAGA complexes purified upon Tra1 *de novo* expression from a strain in which the DUB subunit Sgf11 is MYC-tagged. *spt7-TAP RI-tra1 sgf11-MYC* cells were grown to exponential phase and harvested at different time-points after β-estradiol addition, as indicated (hours). SAGA was purified from a *tra1*Δ strain as a control for the complete loss of Tra1 from SAGA and from a non-tagged strain (no TAP) as a control for background. Silver staining reveals Spt7 and Tra1, which migrate around 150 and 400 kDa, respectively. Anti-HA and anti-MYC Western blotting of Spt7-TAP and Sgf11-MYC in a fraction of the input (Input) and in TAP eluates (TAP) is shown below. An anti-tubulin antibody and Ponceau red staining are used as loading controls. Shown are gels that are representative of four independent experiments, quantified and averaged in (E).

(E) Quantification of the ratio of Tra1 to Spt7 from silver stained gels (top) and of the ratio of Sgf11-MYC to Spt7-TAP from Western blots (bottom). Data points were individually plotted on the graph. Signal intensities were quantified from 2-4 independent experiments.

(F) Working model for the last steps of SAGA assembly. Core subunits (Spt7, Ada1, and TAFs), the HAT module (Gcn5, Ada2, Ada3, and Sgf29), and Spt20 form a pre-assembled complex. The Hsp90 cochaperone TTT catalyses the folding and maturation of Tra1 in the wake of its translation. Tra1 is then anchored to SAGA by the HIT domain from Spt20. Consequently, Tra1 stabilizes the interaction of the DUB (Sgf73, Ubp8, Sgf11, and Sus1) with SAGA to form a mature, fully active multifunctional transcriptional co-activator complex.

Figure 1

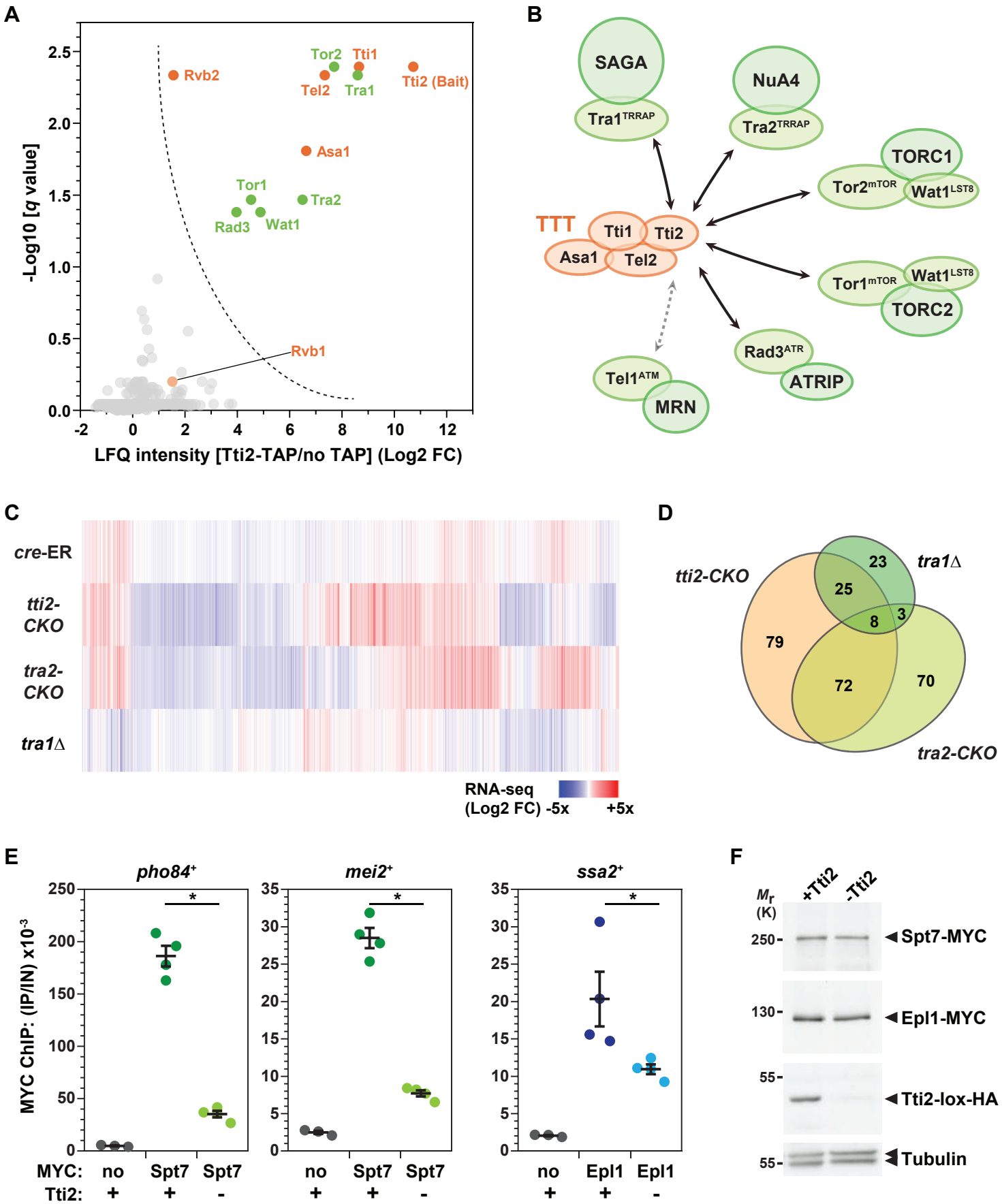
A
-Log10 [q value]
LFQ intensity [Tti2-TAP/no TAP] (Log2 FC)
Rvb2
Tor2
Tti1
Tel2
Tra1
Tti2 (Bait)
Asa1
Tor1
Tra2
Rad3
Wat1
Rvb1
B
SAGA
Tra1TRRAP
NuA4
Tra2TRRAP
TORC1
Tor2mTOR
Wat1LST8
TTT
Tti1
Tti2
Asa1
Tel2
Tor1mTOR
Wat1LST8
TORC2
Rad3ATR
ATRIP
Tel1ATM
MRN
C
cre-ER
tti2-CKO
tra2-CKO
tra1Δ
RNA-seq
(Log2 FC) -5x
+5x
D
tti2-CKO
tra1Δ
tra2-CKO
23
25
8
3
79
72
70
E
pho84+
mei2+
ssa2+
MYC ChIP: (IP/IN) x10-3
MYC:
Tti2:
no
Spt7
Epl1
F
Mr (K)
+Tti2
-Tti2
250
130
55
Spt7-MYC
Epl1-MYC
Tti2-lox-HA
Tubulin

Figure 2

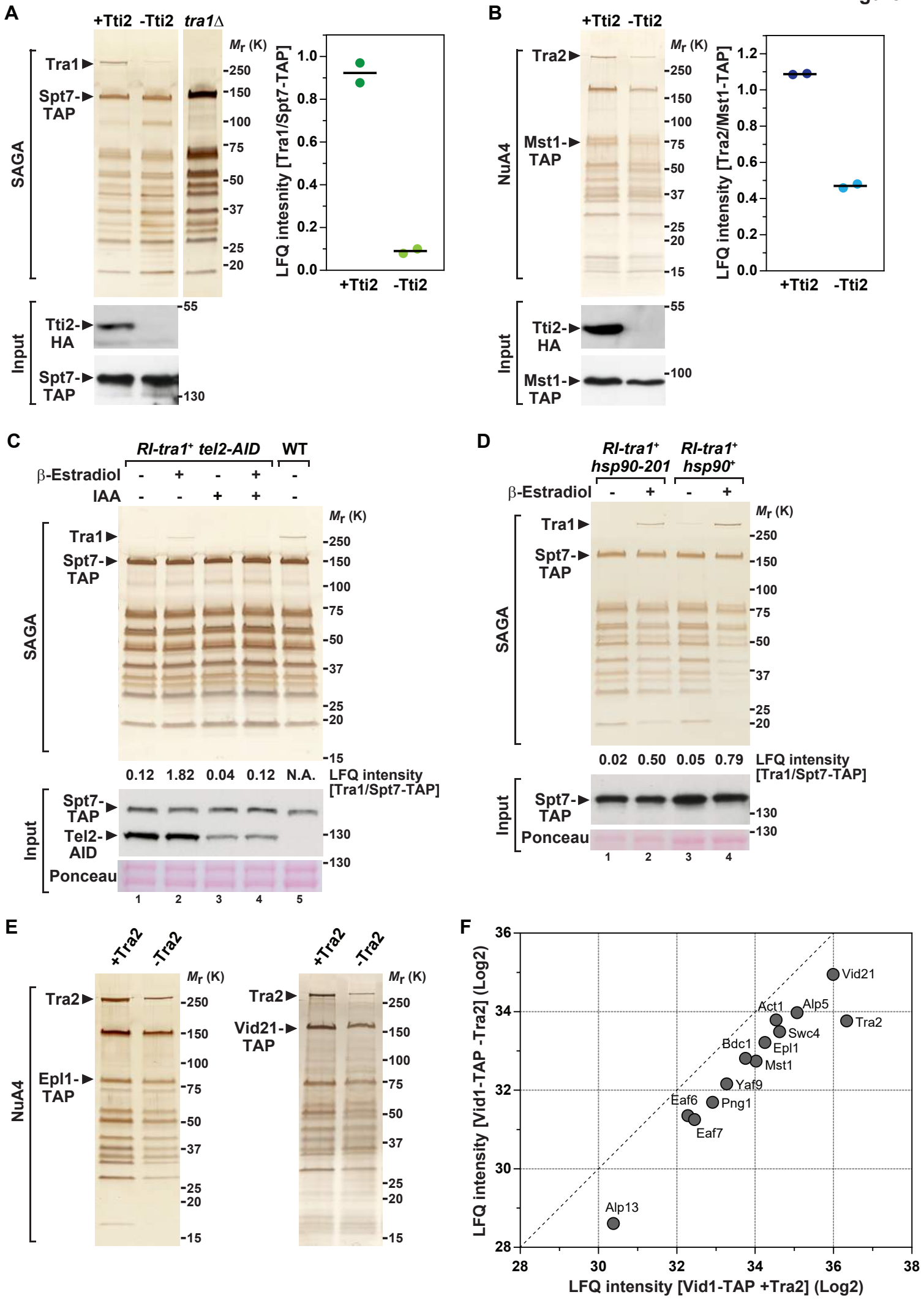
A
+Tti2 -Tti2 tra1Δ
Tra1
Spt7-TAP
SAGA
Mr (K)
250
150
100
75
50
37
25
20
LFQ intesnity [Tra1/Spt7-TAP]
1.0
0.8
0.6
0.4
0.2
0.0
+Tti2 -Tti2
Input
Tti2-HA
Spt7-TAP
55
130
B
+Tti2 -Tti2
Tra2
Mst1-TAP
NuA4
Mr (K)
250
150
100
75
50
37
25
20
15
LFQ intensity [Tra2/Mst1-TAP]
1.2
1.0
0.8
0.6
0.4
0.2
0.0
+Tti2 -Tti2
Input
Tti2-HA
Mst1-TAP
55
100
C
Rl-tra1+ tel2-AID WT
β-Estradiol - + - + -
IAA - - + + -
Tra1
Spt7-TAP
SAGA
Mr (K)
250
150
100
75
50
37
25
20
15
0.12 1.82 0.04 0.12 N.A. LFQ intensity [Tra1/Spt7-TAP]
Input
Spt7-TAP
Tel2-AID
Ponceau
130
130
1 2 3 4 5
D
Rl-tra1+ hsp90-201 Rl-tra1+ hsp90+
β-Estradiol - + - +
Tra1
Spt7-TAP
SAGA
Mr (K)
250
150
100
75
50
37
25
20
0.02 0.50 0.05 0.79 LFQ intensity [Tra1/Spt7-TAP]
Input
Spt7-TAP
Ponceau
130
130
1 2 3 4
E
+Tra2 -Tra2
Tra2
Epl1-TAP
NuA4
Mr (K)
250
150
100
75
50
37
25
20
15
+Tra2 -Tra2
Tra2
Vid21-TAP
Mr (K)
250
150
100
75
50
37
25
20
15
F
LFQ intensity [Vid1-TAP -Tra2] (Log2)
LFQ intensity [Vid1-TAP +Tra2] (Log2)
36
34
32
30
28
28 30 32 34 36 38
Vid21
Act1
Alp5
Tra2
Swc4
Bdc1
Epl1
Mst1
Yaf9
Eaf6
Png1
Eaf7
Alp13

Figure 3

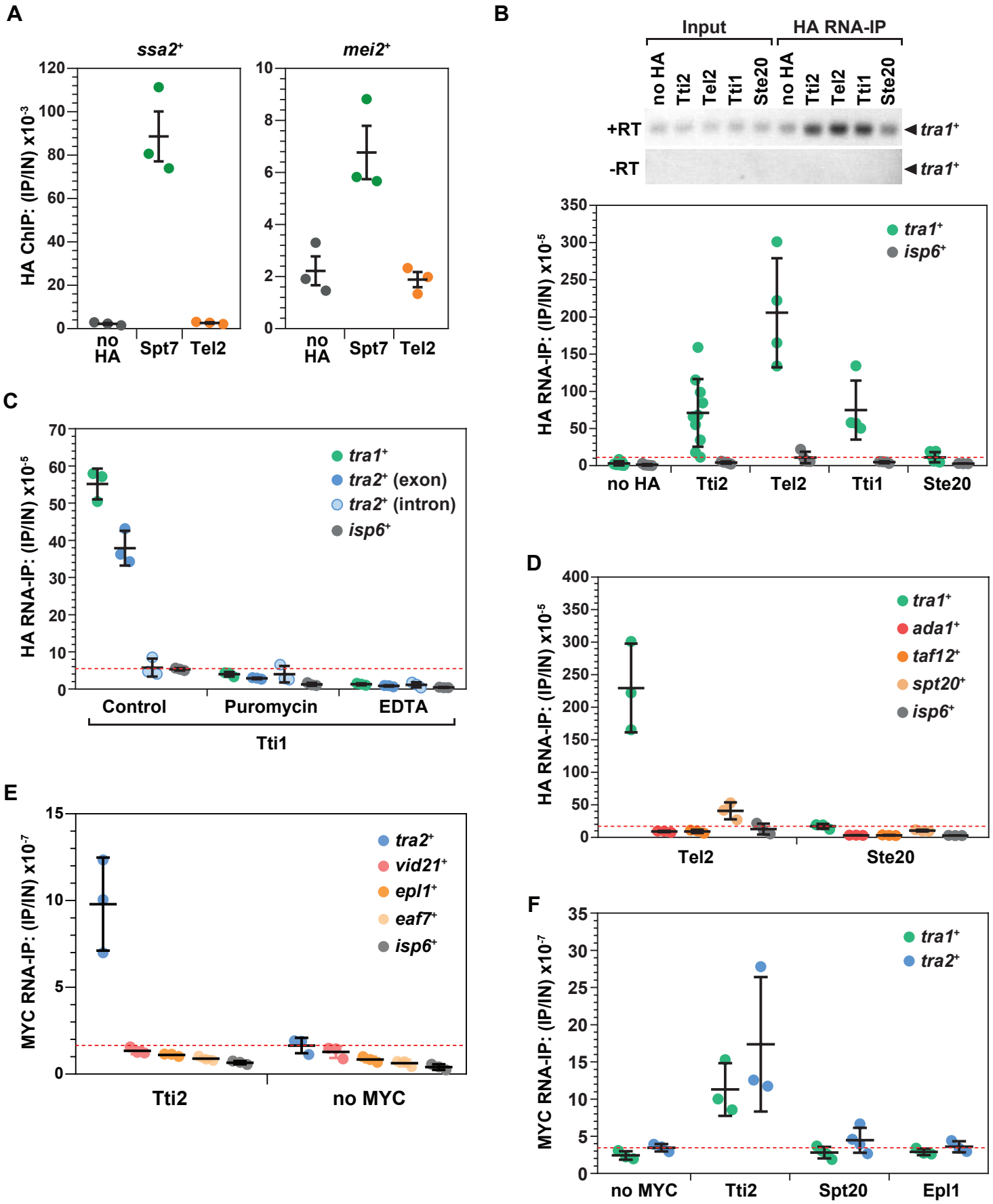
A
ssa2+
mei2+
HA ChIP: (IP/IN) x10-3
no HA
Spt7
Tel2
B
Input
HA RNA-IP
no HA
Tti2
Tel2
Tti1
Ste20
+RT
-RT
tra1+
HA RNA-IP: (IP/IN) x10-5
isp6+
C
tra2+ (exon)
tra2+ (intron)
Control
Puromycin
EDTA
Tti1
D
ada1+
taf12+
spt20+
E
MYC RNA-IP: (IP/IN) x10-7
vid21+
epl1+
eaf7+
no MYC
F
Spt20
Epl1

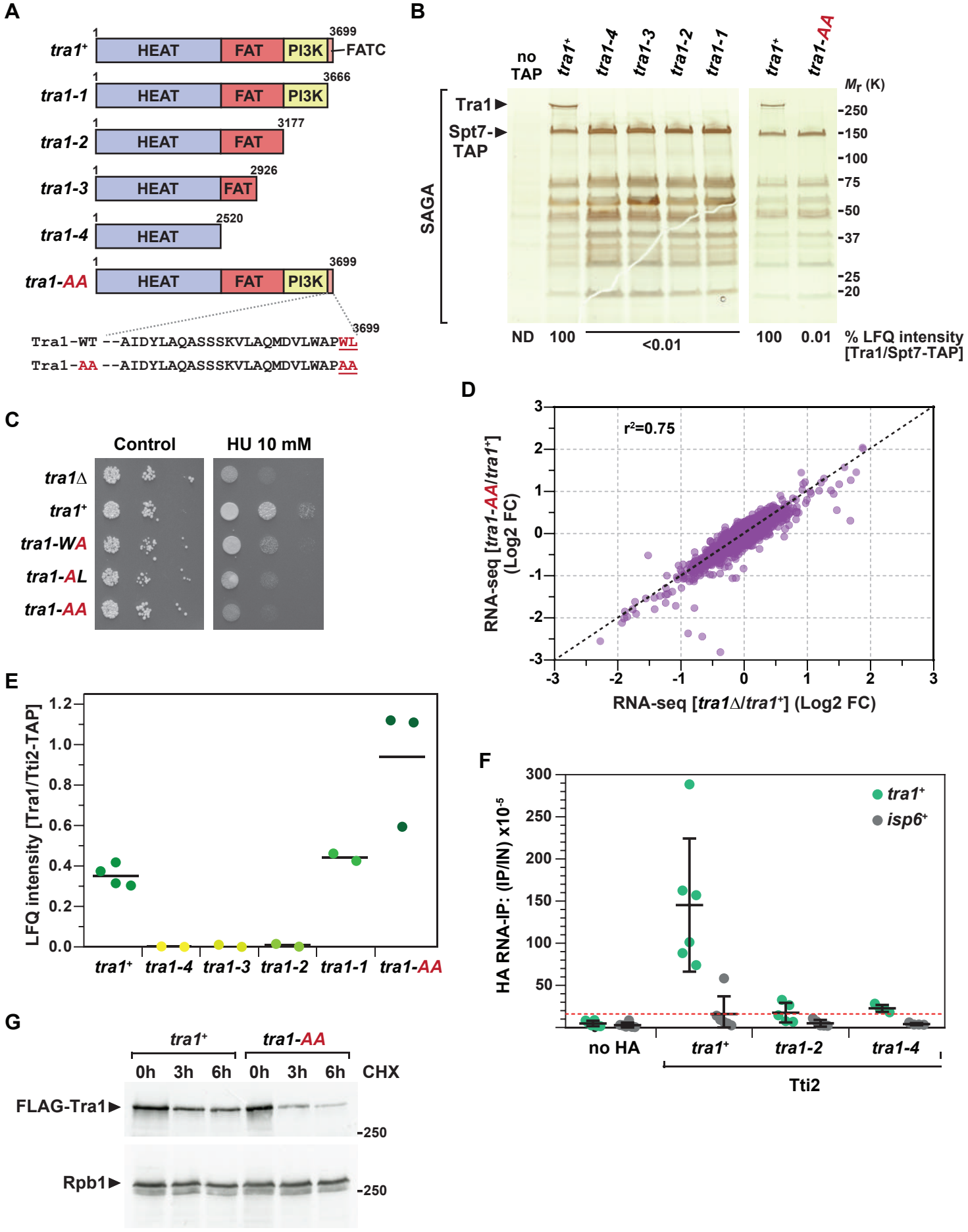
A
tra1+
HEAT
FAT
PI3K
FATC
1
3699
tra1-1
3666
tra1-2
3177
tra1-3
2926
tra1-4
2520
tra1-AA
Tra1-WT --AIDYLAQASSSKVLAQMDVLWAPWL
Tra1-AA --AIDYLAQASSSKVLAQMDVLWAPAA
B
no TAP
tra1+
tra1-4
tra1-3
tra1-2
tra1-1
tra1-AA
Mr (K)
Tra1
Spt7-TAP
SAGA
-250
-150
-100
-75
-50
-37
-25
-20
ND
100
<0.01
100
0.01
% LFQ intensity [Tra1/Spt7-TAP]
C
Control
HU 10 mM
tra1Δ
tra1+
tra1-WA
tra1-AL
tra1-AA
D
r2=0.75
RNA-seq [tra1-AA/tra1+] (Log2 FC)
RNA-seq [tra1Δ/tra1+] (Log2 FC)
E
LFQ intensity [Tra1/Tti2-TAP]
tra1+
tra1-4
tra1-3
tra1-2
tra1-1
tra1-AA
F
HA RNA-IP: (IP/IN) x10-5
tra1+
isp6+
no HA
tra1+
tra1-2
tra1-4
Tti2
G
tra1+
tra1-AA
0h
3h
6h
0h
3h
6h
CHX
FLAG-Tra1
Rpb1
-250
-250

Figure 5

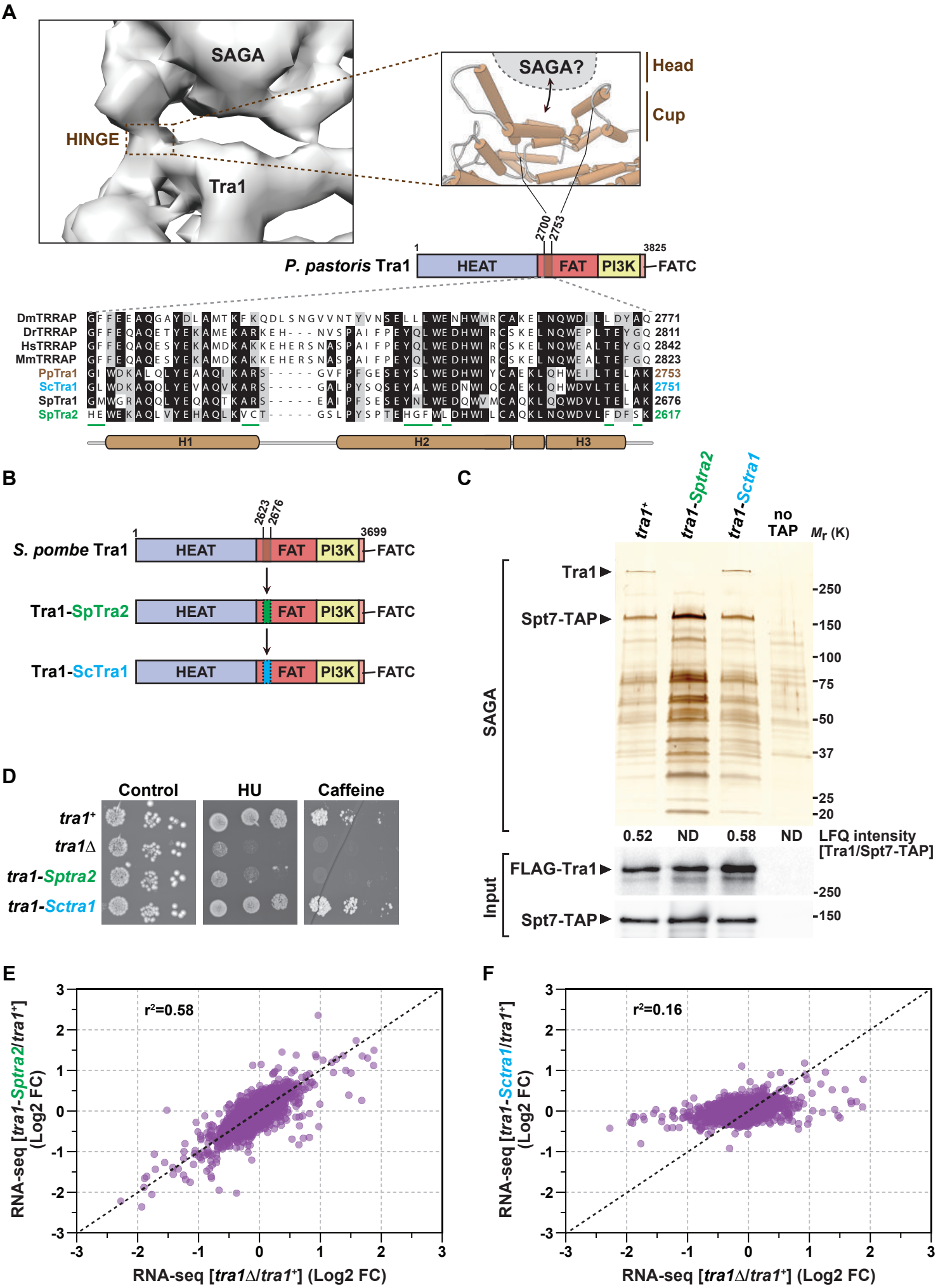
A
SAGA
HINGE
Tra1
SAGA?
Head
Cup
2700
2753
1
3825
P. pastoris Tra1
HEAT
FAT
PI3K
FATC
DmTRRAP
DrTRRAP
HsTRRAP
MmTRRAP
PpTra1
ScTra1
SpTra1
SpTra2
H1
H2
H3
B
2623
2676
S. pombe Tra1
Tra1-SpTra2
Tra1-ScTra1
C
tra1+
tra1-Sptra2
tra1-Sctra1
no TAP
Mr (K)
Tra1
Spt7-TAP
SAGA
-250
-150
-100
-75
-50
-37
-25
-20
0.52
ND
0.58
ND
LFQ intensity [Tra1/Spt7-TAP]
Input
FLAG-Tra1
Spt7-TAP
D
Control
HU
Caffeine
tra1+
tra1Δ
tra1-Sptra2
tra1-Sctra1
E
r2=0.58
RNA-seq [tra1-Sptra2/tra1+] (Log2 FC)
RNA-seq [tra1Δ/tra1+] (Log2 FC)
F
r2=0.16
RNA-seq [tra1-Sctra1/tra1+] (Log2 FC)
RNA-seq [tra1Δ/tra1+] (Log2 FC)

Figure 6

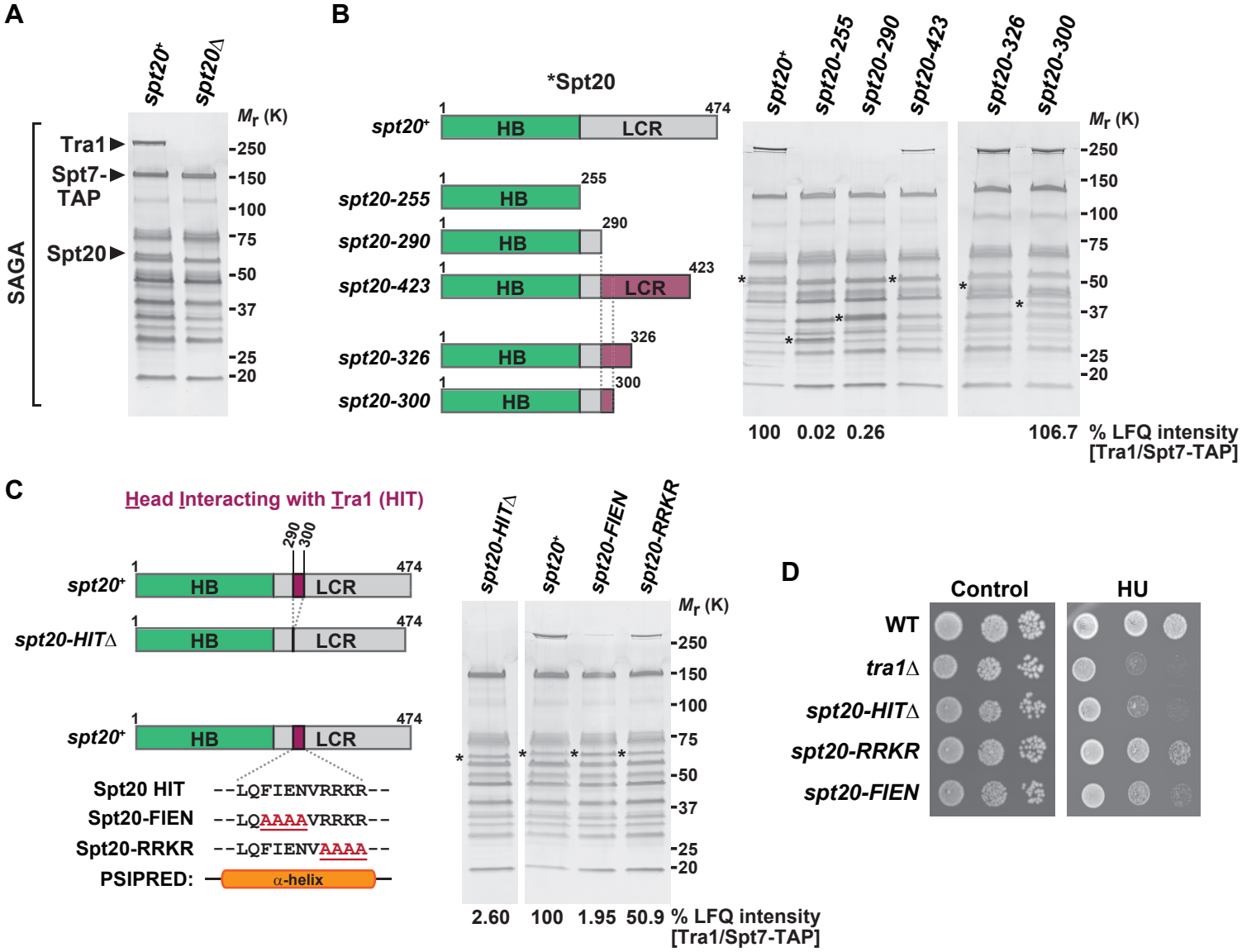
A
spt20+
spt20Δ
Mr (K)
Tra1
Spt7-TAP
Spt20
SAGA
250
150
100
75
50
37
25
20
B
*Spt20
spt20+
HB
LCR
1
474
spt20-255
255
spt20-290
290
spt20-423
423
spt20-326
326
spt20-300
300
spt20-255
spt20-290
spt20-423
spt20-326
spt20-300
100 0.02 0.26 106.7 % LFQ intensity [Tra1/Spt7-TAP]
C
Head Interacting with Tra1 (HIT)
290
300
spt20-HITΔ
Spt20 HIT --LQFIENVRRKR--
Spt20-FIEN --LQAAAAVRRKR--
Spt20-RRKR --LQFIENVAAAA--
PSIPRED:
α-helix
spt20-FIEN
spt20-RRKR
2.60 100 1.95 50.9 % LFQ intensity [Tra1/Spt7-TAP]
D
Control
HU
WT
tra1Δ
spt20-HITΔ
spt20-RRKR
spt20-FIEN
E
r²=0.35
RNA-seq [spt20-HITΔ/WT] (Log2 FC)
RNA-seq [spt20Δ/WT] (Log2 FC)
F
r²=0.44
RNA-seq [tra1Δ/WT] (Log2 FC)
G
r²=0.62
RNA-seq [tra1-Sptra2/tra1+] (Log2 FC)
H
GST
GST-HIT
Coomassie
Input
no FLAG
tra1+
tra1-Sptra2
tra1-Sctra1
FLAG-Tra1
Pull-down
GST
GST-HIT

Figure 7

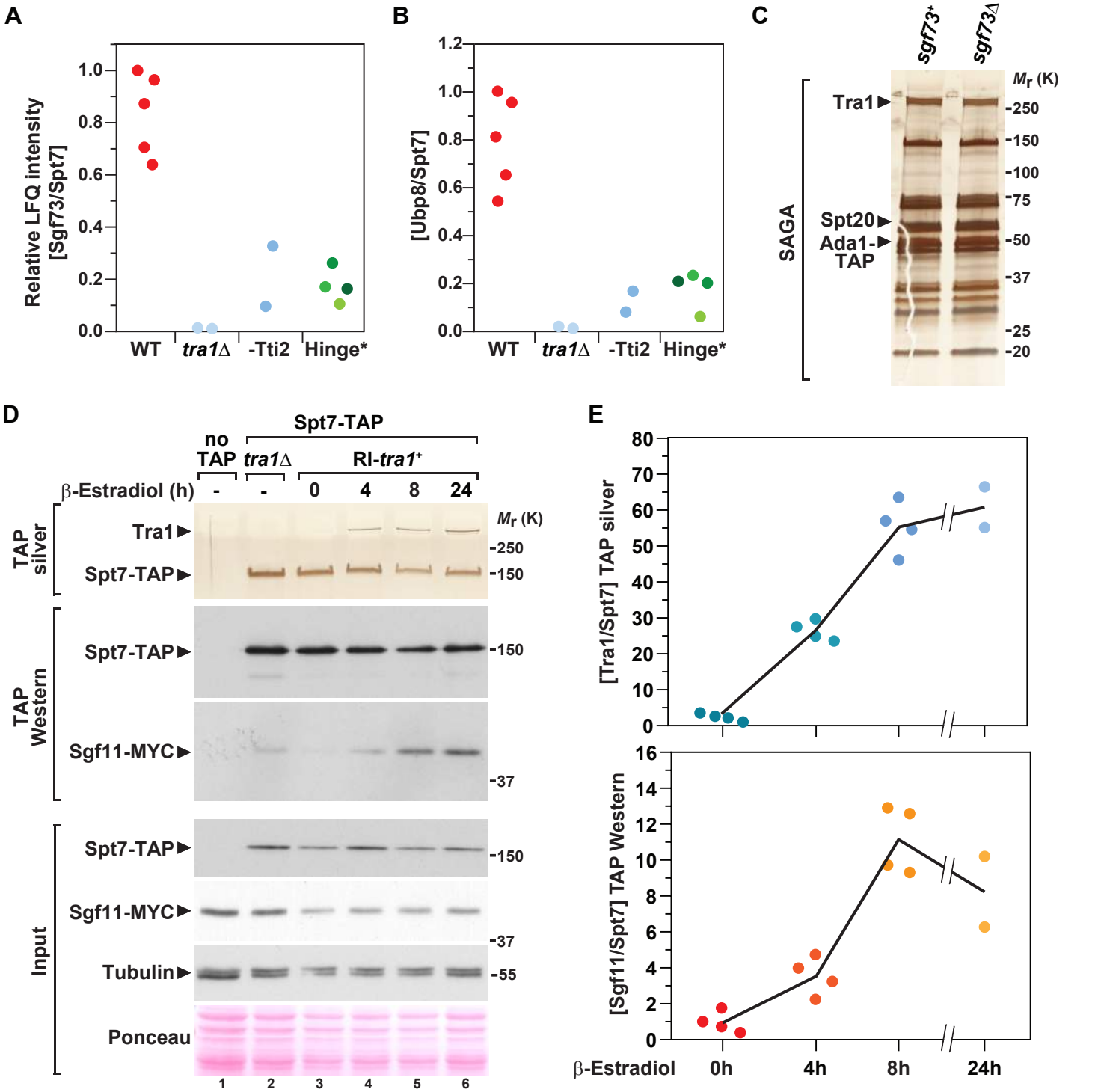
A
Relative LFQ intensity [Sgf73/Spt7]
1.0
0.8
0.6
0.4
0.2
0.0
WT
tra1Δ
-Tti2
Hinge*
B
[Ubp8/Spt7]
1.2
1.0
0.8
0.6
0.4
0.2
0.0
WT
tra1Δ
-Tti2
Hinge*
C
sgf73+
sgf73Δ
Mr (K)
Tra1
Spt20
Ada1-TAP
SAGA
250
150
100
75
50
37
25
20
D
Spt7-TAP
no TAP
tra1Δ
RI-tra1+
β-Estradiol (h)
-
-
0
4
8
24
TAP silver
Tra1
Spt7-TAP
TAP Western
Spt7-TAP
Sgf11-MYC
Input
Spt7-TAP
Sgf11-MYC
Tubulin
Ponceau
Mr (K)
250
150
150
37
150
37
55
1
2
3
4
5
6
E
[Tra1/Spt7] TAP silver
80
70
60
50
40
30
20
10
0
[Sgf11/Spt7] TAP Western
16
14
12
10
8
6
4
2
0
β-Estradiol
0h
4h
8h
24h
F
HAT
CORE
Spt20
TTT
Tra1
Tra1
TTT
5'
3'
tra1+ mRNA
HAT
CORE
Spt20
Tra1
DUB
SAGA
HAT
CORE
DUB
Spt20
Tra1